MTL TR 90-6

AD-A220 428

AD

FRACTURE MECHANISM MAPS FOR ADVANCED STRUCTURAL CERAMICS PART I: METHODOLOGY AND HOT-PRESSED SILICON NITRIDE RESULTS

GEORGE D. QUINN
CERAMICS RESEARCH BRANCH

February 1990

US ARMY
LABORATORY COMMAND
MATERIALS TECHNOLOGY LABORATORY

U.S. ARMY MATERIALS TECHNOLOGY LABORATORY
Watertown, Massachusetts 02172-0001

The findings in this report are not to be construed as an official Department of the Army position, unless so designated by other authorized documents.

Mention of any trade names or manufacturers in this report shall not be construed as advertising nor as an official indorsement or approval of such products or companies by the United States Government.

DISPOSITION INSTRUCTIONS

Destroy this report when it is no longer needed.
Do not return it to the originator.

UNCLASSIFIED

SECURITY CLASSIFICATION OF THIS PAGE *(When Data Entered)*

REPORT DOCUMENTATION PAGE		READ INSTRUCTIONS BEFORE COMPLETING FORM
1. REPORT NUMBER MTL TR 90-6	2. GOVT ACCESSION NO.	3. RECIPIENT'S CATALOG NUMBER
4. TITLE *(and Subtitle)* FRACTURE MECHANISM MAPS FOR ADVANCED STRUCTURAL CERAMICS. PART I: METHODOLOGY AND HOT-PRESSED SILICON NITRIDE RESULTS		5. TYPE OF REPORT & PERIOD COVERED Final Report 6. PERFORMING ORG. REPORT NUMBER
7. AUTHOR(s) George D. Quinn		8. CONTRACT OR GRANT NUMBER(s)
9. PERFORMING ORGANIZATION NAME AND ADDRESS U.S. Army Materials Technology Laboratory Watertown, Massachusetts 02172-0001 SLCMT-EMC		10. PROGRAM ELEMENT, PROJECT, TASK AREA & WORK UNIT NUMBERS D/A Project: 1L162105.AH84
11. CONTROLLING OFFICE NAME AND ADDRESS U.S. Army Laboratory Command 2800 Powder Mill Road Adelphi, Maryland 20783-1145		12. REPORT DATE February 1990 13. NUMBER OF PAGES 30
14. MONITORING AGENCY NAME & ADDRESS *(if different from Controlling Office)*		15. SECURITY CLASS. *(of this report)* Unclassified 15a. DECLASSIFICATION/DOWNGRADING SCHEDULE

16. DISTRIBUTION STATEMENT *(of this Report)*

Approved for public release; distribution unlimited.

17. DISTRIBUTION STATEMENT *(of the abstract entered in Block 20, if different from Report)*

18. SUPPLEMENTARY NOTES

19. KEY WORDS *(Continue on reverse side if necessary and identify by block number)*

Ceramics	Fracture mechanics
Silicon nitride	Fracture maps
Powders	Stress rupture
Hot pressing	Creep rupture

20. ABSTRACT *(Continue on reverse side if necessary and identify by block number)*

(SEE REVERSE SIDE)

DD FORM 1 JAN 73 1473 EDITION OF 1 NOV 65 IS OBSOLETE

UNCLASSIFIED

SECURITY CLASSIFICATION OF THIS PAGE *(When Data Entered)*

Block No. 20

ABSTRACT

The static fatigue behavior of advanced structural ceramics can be controlled by a variety of failure mechanisms. A fracture mechanism map can define the stress-temperature regimes where the different mechanisms are dominant. The static fatigue resistance of a hot-pressed silicon nitride with magnesia sintering aid is limited by slow crack growth or creep fracture, depending upon the specific stress-temperature conditions. The flexural fracture map is considerably refined relative to earlier versions, and in conjunction with available tension data, was used to create a tension fracture map. The fracture map brings together the findings of a number of studies and can be appreciated by materials scientists and engineers.

CONTENTS

	Page
INTRODUCTION	1
MATERIAL	2
EXPERIMENTAL PROCEDURE	2
RESULTS	4
DISCUSSION	12
COMPARISON OF TENSION TO FLEXURE RESULTS	19
CONCLUSIONS	25
REFERENCES	26

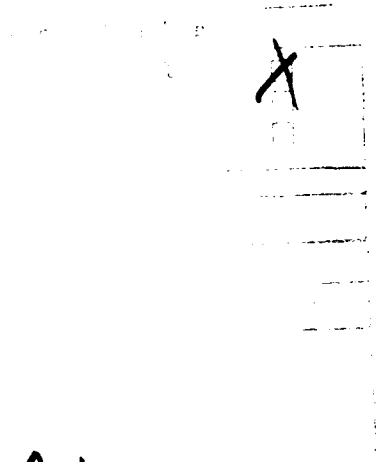

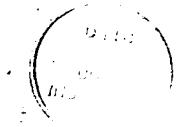

A-1

INTRODUCTION

Static fatigue and stress rupture studies for advanced structural ceramics have often examined one mechanism of time-dependent failure. In the 1970s, work was focussed on slow crack growth (SCG) from preexisting flaws in silicon nitrides and carbides. These flaws limit the fast fracture strength and are typically inclusions, pores, machining damage, or even artificially implanted Knoop defects. Reference 1 is a review paper and bibliography of such work.

More recent studies have been concerned with creep crack growth or creep fracture. At certain stress-temperature conditions, creep deformations can blunt preexisting defects. Excessive creep deformations may, however, lead to microcrack nucleation, intergranular growth, and coalescence leading to fracture. Although both SCG and creep fracture mechanisms have intergranular crack growth stages, the key distinction is that slow crack growth emanates from preexisting flaws, with creep deformations and microcracking confined to the crack tip. Creep fracture, on the other hand, has bulk deformation and microcracking and may not necessarily involve preexisting flaws. Alumina is often used in these more recent studies because of its lower cost and its suitability as a model material.[2-7]

Alternative static fatigue mechanisms can be operative in advanced ceramics such as stress corrosion or surface pitting. A convenient scheme to identify the stress-temperature regimes where the respective static fatigue mechanisms are dominant is the fracture mechanism map, as first suggested by Wray[8] for a stainless steel. Fracture maps were further developed by Fields, Weerasooriya and Ashby.[9] Gandhi and Ashby[10] applied the approach to a range of ceramics, including several speculative maps for advanced structural ceramics that were available in the early 1970s.

This report presents stress rupture results and a fracture map for a hot-pressed silicon nitride (HPSN). This approach has also been applied to a more modern sintered silicon nitride.[11] Preliminary work on the HPSN culminated in empirical procedures to generate a fracture mechanism map.[12-14]

1. QUINN, G. D. *Ceram. Eng. Sci. Proc.* v. 3, no. 1-2, 1982, p. 77.
2. WIEDERHORN, S. M., HOCKEY, B. J., KRAUSE, R. F., and JAKUS, K. *J. Mat. Sci.* v. 21, 1986, p. 810.
3. JOHNSON, S. M., DALGLEISH, B. J., and EVANS, A. G. *J. Am. Ceram. Soc.* v. 67, 1984, p. 759.
4. BLUEMENTHAL, W., and EVANS, A. G. *J. Am. Ceram. Soc.* idem, p. 751.
5. OKADA, T., and SINES, G. *J. Amer. Ceram. Soc.* v. 66, no. 10, 1983, p. 719.
6. ROBERTSON, A. G., and WILKINSON, D. S. Fracture Mechanics of Ceramics. R. C. Bradt, A. G. Evans, D. P. H. Hasselman, and F. Lange, ed., Plenum Press, New York, v. 7, 1986, p. 311.
7. HASSELMAN, D. P. H., VENKATESWAREN, A., and SHIH, C. *Surfaces and Interfaces in Ceramic and Ceramic Metal Systems.* Materials Science Research, J. Pask, and E. Evans, ed., Plenum Press, New York, v. 14, 1981, p. 323.
8. WRAY, P. J. *J. Appl. Phys.* v. 40, 1969, p. 4018.
9. FIELDS, R. J., WEERASOORIYA, T., and ASHBY, M. F. *Met. Trans. A.* v. 11A, 1980, p. 333.
10. GANDHI, C., and ASHBY, M. *Acta. Met.* v. 27, 1979, p. 1565.
11. QUINN, G. D., and BRAUE, W. R. Submitted to J. Mat. Sci., 1990.
12. QUINN, G. D *Methods for Assessing the Structural Reliability of Brittle Materials.* S. W. Freiman and C. M. Hudson, ed., American Society of Testing and Materials, Philadelphia, Pennsylvania, ASTM STP 844, 1984, p. 177.
13. QUINN, G. D. *Ceram. Eng. Sci. Proc.* v. 5, no. 7-8, 1984, p. 596.
14. QUINN, G. D. Fracture Mechanics of Ceramics. R. Bradt, A. G. Evans, D. Hasselman, and F. Lange, ed., Plenum Press, New York, v. 8, 1986, p. 319.

MATERIAL

Hot-pressed silicon nitride, grade NC 132,* was fabricated with a magnesia sintering aid and has been characterized previously.[14-18] Principle contaminants were determined by emission spectroscopy to be aluminum (0.28 wt%), cobalt (0.17%), iron (0.32%), and titanium (0.12%). Tungsten was also detected at the level of several percent, but some of this was pickup from the pulverizing apparatus. All results herein were obtained with specimens from two 150 mm x 150 mm x 25 mm billets (A and P) which had consistent static fatigue behavior. Flexure specimens were either 2.1 mm x 2.8 mm x 51 mm (as-machined experiments) or 2.3 mm x 3.6 mm x 51 mm (artificial flaw experiments). Five hundred and fifty specimens in all were prepared.

EXPERIMENTAL PROCEDURE

All experiments were performed in four-point flexure. While it is generally agreed that direct tension testing is to be preferred, such testing capability was not available for this program. Indeed, the high number of specimens required to develop a fracture map, and the very long duration of the experiments often necessary (> 1 year), mitigate against direct tension testing. The state-of-the-art of ceramics testing is evolving at the present time and future studies based upon complimentary flexure and direct tension testing will become more common.

The room temperature fast fracture strength was evaluated to serve as a baseline strength and to identify the typical strength limiting flaws. Four-point fixture with fixed loading pins and 30.5 mm x 15.2 mm spans and a 0.5 mm/min crosshead rate were used. All testing was in air with ambient humidity and temperature levels.

Elevated temperature flexure was performed with hot-pressed silicon carbide fixtures with spans of either 19.0 mm x 38.0 mm or 20.0 mm x 40.0 mm; load bearings were fixed.† All stress rupture experiments were done with dead-weight loading applied into fifteen test furnaces, described previously.[18,19] The individual furnaces were all consistent within 5°C. Errors in stress, due to the loading system, were kept to less than two percent. The furnaces were allowed to sit at temperature for five minutes prior to loading to let the furnace stabilize. Loading was done manually by lowering a lab jack such that the weights were transmitted onto the loading lever in five seconds. Elapsed time was measured from the instant full load was applied, and failure time was noted by a timer on each furnace. The instant a specimen failed, the furnace power was automatically shut off so that primary fracture surfaces could be preserved.

Stress rupture data in this report is represented on log time axes that begin at 0.001 hour (3.6 seconds). The exact manner of loading surely will affect experiments of such

*Norton Company, Worcester, Mass.

†Preliminary experiments with rolling bearing high temperature fixtures have had partial success, but were not used for this study. The rolling action is necessary to eliminate unwanted friction constraints in the specimen which cause an error in stress.

15. TORTI, M. L. Ceramics for High Performance Applications III, Reliability. E. Lenoe, R. Katz, and J. Burke, ed., Plenum Press, New York, 1983, p. 261.

16. QUINN, G. D. Ceramic Materials and Components for Engines. W. Bunk and H. Hausner, ed., Deutsche Keramische Gesselschaft, Berlin, Germany, 1986, p. 931.

17. QUINN, G. D., and QUINN, J. B. Fracture Mechanics of Ceramics. R. Bradt, A. Evans, D. Hasselman, and F. Lange, ed., Plenum Press, New York, v. 6, 1983, p. 603.

18. QUINN, G. D. *Characterization of Turbine Ceramics After Long-Term Environmental Exposure.* U.S. Army Materials Technology Laboratory, AMMRC TR 80-15, 1980.

19. QUINN, G. D. *Guide to the Construction of A Simple 1500°C Test Furnace.* U.S. Army Materials Technology Laboratory, AMMRC TN 77-4, August 1977, republished as TR 83-1, January 1983.

duration and make them less accurate than longer experiments. Applied stresses were computed on the basis of the elastic beam formula for the maximum tensile stress on the tensile surface. Nearly all origins of failure were from this region. In many instances, large cracks grew and extended into the bulk. This would surely alter the stress state, but it can be demonstrated, using any one of the crack growth formulations, that the crack size is small over the major portion of the lifetime of the specimen. Creep relaxations were present in many of the specimens where the elastic formulation for stress was an overestimate.

The state of stress in a flexure specimen is a strong function of time and temperature if creep occurs. A number of authors have attempted to analytically correct or adjust their results to correct for creep relaxations, but such work has been hampered by the number of assumptions involved, particularly in the choice of constitutive equations. Primary creep can be significant,[20-24] the secondary creep rate is often nonlinear with time,[21,25] rates in tension and compression are significantly different,[20,23,26] viscoelasticity can be present,[25] and devitrification[2,27] and oxidation gradients at different rates through the specimen thickness[28,29] are complicating factors. Creep microcracking will alter the specimen compliance[30] and accumulated tension damage can distort the measured creep exponents.[30,31] The secondary creep rate is often not achieved in hundreds or even thousands of hours.[25,32] Several of these phenomena are well illustrated for a siliconized silicon carbide,[33] wherein it was shown that the neutral axis of the flexure specimen had migrated drastically. These phenomena are often very significant and will cause great variability in the constitutive equations through the thickness of the specimen, especially if more than one phenomena is operative. Another good example is from Wiederhorn et al.,[2] wherein a myriad of constitutive equations become pertinent in an aluminum oxide with a glass boundary phase that devitrified at different rates from the compression to the tension side. In such cases, Wilkinson[27] concluded that it is "virtually impossible to extract meaningful creep data from tests performed in bending." Attempting to model flexural creep with simplified constitutive equations and then adjusting parameters to get a best fit to the data is a curve-fitting exercise. Jakus and Wiederhorn[32] point out that erroneous creep exponents can be an artifact of flexure testing. Furthermore, frictional constraints of fixed-knife edges and contact point tangency shifts of specimens that have crept more than a few tenths of a percent strain have been completely ignored. It must, therefore, be concluded that, in many instances, detailed analyses of flexural creep data are not warranted.

All stresses in this study were left in terms of the applied elastic stresses, which are certainly correct for specimens with no creep and for short times even if there is creep. Clearly, direct tension and compression testing are preferred for future studies. Jakus and Wiederhorn[32] have reached the same conclusion.

20. COHRT, H., GRATHWOHL, G., and THUMMLER, F. *Res. Mech. Let.* v. 1, 1981, p. 159.
21. GRATHWOHL, G. Deformation of Ceramic Materials, II. R. Tressler and R. Bradt, ed., Plenum Press, New York, 1984, p. 573.
22. FETT, T. *J. Mat. Sci. Let.* v. 6, 1987, p. 967.
23. FETT, T., and MUNZ, D. *Int. J. High Tech. Ceram.* v. 4, 1988, p. 281.
24. FETT, T., KELLER, K., and MUNZ, D. *J. Mat. Sci.* v. 23, 1988, p. 467.
25. ARONS, R., and TIEN, J. *J. Mat. Sci.* v. 15, 1980, p. 2046.
26. CARROLL, D. F., CHUANG, T. J., and WIEDERHORN, S. M. *Ceram. Eng. Sci. Proc.* v. 9, no. 7-8, 1988, p. 635.
27. WILKINSON, D. S. *J. Amer. Ceram. Soc.* v. 71, 1988, p. 562.
28. DAS, G., MENDIRATTA, M. G., and CORNISH, G. R. *J. Mat. Sci.* v. 17, 1982, p. 2486.
29. GRATHWOHL, G., and THUMMLER, F. *J. Mat. Sci.* v. 13, 1978, p. 1177.
30. VENKATESWAREN, A., and HASSELMAN, D. P. H. *J. Mat. Sci.* v. 16, 1981, p. 1627.
31. ROSENFIELD, A. R., DUCKWORTH, W. H., and SHETTY, D. K. *J. Amer. Ceram. Soc.* v. 68, 1985, p. 485.
32. JAKUS, K., and WIEDERHORN, S. *J. Amer. Ceram. Soc.* v. 71, no. 10, 1988, p. 832.
33. WIEDERHORN, S., CHUCK, L., FULLER, E., and TIGHE, N. *Tailoring of Multiphase and Composite Ceramics.* Materials Science Research, R. E. Tressler, G. L. Mecholsky, C. G. Pantano, and R. E. Newnham, ed., Plenum Press, New York, v. 20, 1986, p. 755.

Creep deformations were not measured during the experiments, but final deformations were used to compute an apparent strain-at-failure ε_f from the formula:

$$\varepsilon_f = 4\ t\ v\ /\ L^2 \qquad (1)$$

where t is specimen thickness, v is the midspan deflection relative to the inner load pins, and L is the outer span length. Even this formula is an oversimplification, since it assumes the strains in compression and tension are equal.

Specimens were tested in either the as-machined state or with an implanted artificial flaw. In the latter case, a Knoop indentation was made on a polished surface, which created not only the hardness impression, but a subsurface semielliptical crack, as depicted in Figure 1. The purpose was to create a flaw large enough to guarantee it was the severest in the specimen and to precisely control its size and location. No provision was made to remove the residual indentation stresses since it was originally assumed they would be annealed during furnace heating (an unavoidable step) or during the customary five-minute soak prior to load application. An indentation load of 15.7 N was used on 240 HPSN specimens indicated in this report. (Experiments with alternative loads are reported in Reference 17.) This load created a semielliptical surface flaw of 50 microns depth which limited the room temperature strength to 370 MPa. Such artificial flaws were more severe than the natural defects which limited strength to 500 MPa to 1000 MPa.

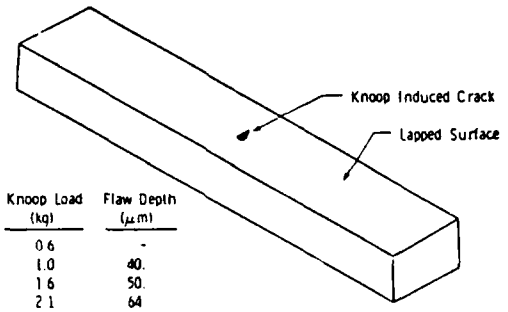

Knoop Load (kg)	Flaw Depth (μm)
0.6	-
1.0	40.
1.6	50.
2.1	64
2.6	70.
3.5	85

Figure 1. Flexure specimen with an artificially implanted semielliptical surface defect. The flaw depth for HPSN varies with the Knoop indentation load. A load of 15.7 N (1.6 kg) was used for the specimens in this study.

RESULTS

The average flexure strength of 16 specimens from billet A was 909 MPa with a 67 MPa standard deviation. The Weibull two parameter modulus (m) from a least squares analysis was 16.6 (see Figure 2). Machining damage was the most common strength limiting defect (~20 μm deep), with some tungsten carbide or silicide inclusions as well, as shown in the labelled Weibull plot in Figure 2. Ten specimens from billet P (which was prepared from the same powder lot) had a mean strength of 872 MPa, a 54 MPa standard deviation, an m of 19.1, and identical strength limiting defects. The flexure strength of specimens from the two billets are quite consistent. The **combined** mean strength is 895 MPa. The Weibull modulus, is 17.2 and the characteristic strength of the bend specimen is 923 MPa. The characteristic strength for a volume of 1 mm^3 would be 988 MPa. Subsequent stress rupture testing confirmed that the static fatigue behavior of the two billets was identical as well.

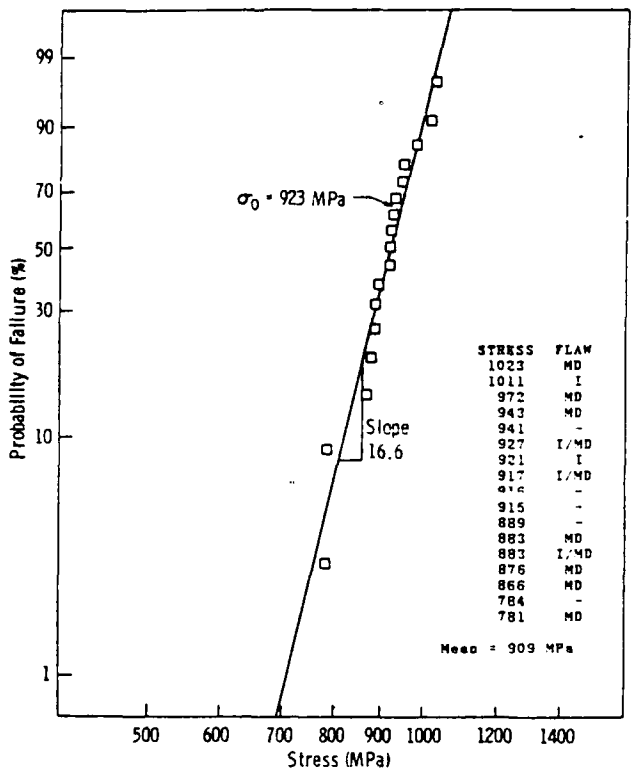

Figure 2. Room temperature flexure strength of the as-machined HPSN specimens. The insert lists the individual strength data and the strength limiting flaw. MD denotes machining damage; I, inclusion; I/MD, an inclusion or machining damage; and -, uncertain.

Figure 3 presents the stress rupture outcomes for the as-machined HPSN specimens. The scatter in time-to-failure is remarkably small over the 1100°C to 1400°C range. Points with arrows are either specimens that failed on loading or specimens which survived intact. A power law relationship exists between crack velocity (v) and stress intensity (K_I):[34,35]

$$v = A K_I^N \exp(-Q_{scg}/RT) \quad (2)$$

where N and A are constants, Q_{scg} is the activation energy of slow crack growth, R is the gas constant, and T is absolute temperature. It can be shown that the stress rupture data should be linear on a log stress-log time graph, as shown in Figure 3.[36,37] The inverse negative slope of the stress rupture curves is the slow crack growth exponent, N. The values of N, from Figure 3, are 29.6, 19.5, 12.8, 9.9, and 9.2 for 1000°C, 1100°C, 1200°C, 1300°C, and 1400°C, respectively. These exponents are upper limits since the elastic stresses are overestimates for the longer duration experiments due to creep relaxation of the stress.

34. CHARLES, R. J. *J. Appl. Phys.* v. 29, no. 12, 1958, p. 1657.
35. EVANS, A. G., RUSSELL, L. R., and RICHERSON, D. W. *Met. Trans. A.* v. 6A, 1975, p. 707.
36. DAVIDGE, R., McLAREN, J., and TAPPIN, G. *J. Mat. Sci.* v. 8, 1973, p. 1699.
37. RITTER, J., Jr. Fracture Mechanics of Ceramics. R. Bradt, D. Hasselman, and F. Lange, ed., Plenum Press, New York, v. 4, 1978, p. 667.

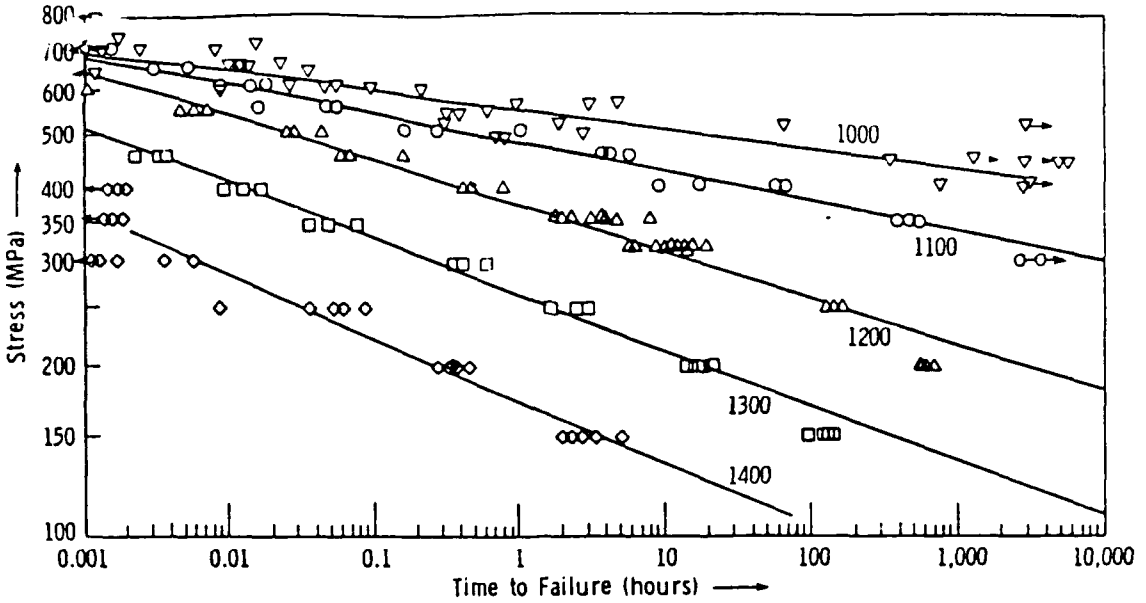

Figure 3. Flexural stress rupture results for as-machined HPSN. Temperatures were from 1000°C to 1400°C, as shown. All stresses are elastic stresses.

The results also plot very well on a semilog format of stress versus log time, as discussed in Reference 14. From 1100°C to 1400°C, the data is well represented by the relationship:

$$t_f = 3.09 \times 10^{-21} \exp (180/RT) \exp (-0.037\ \sigma_a) \quad (3)$$

where t_f is the time-to-failure in hours and σ_a is the applied elastic stress in MPa. The apparent activation energy is 180 kcal/gmole.

The remarkable reproducibility of stress rupture results for this particular grade HPSN is illustrated in Figure 4. There is excellent agreement among the flexure results despite different source billets, specimen sizes, specimen preparations, test fixtures, and laboratories involved.[14,17,38-42] This helps explain why this vintage HPSN has gained wide acceptance as a model structural ceramic. More stress rupture data exists for this material than for any other high performance ceramic. The variation in median time-to-failure of the different studies is, at the most, a factor of 10 and can be traced to billet-to-billet differences or variability in the baseline strength. Systematic differences in the baseline strength from billet to billet are known to exist in this material.[17,43-48] The variability in absolute times-to-failure is probably related to the precise MgO/SiO_2 molar ratio of the starting powders.[45] The fatigue resistance parameters are nonetheless very consistent.[17,38,49]

38. QUINN, G. D., and SWANK, L. *Comm. Amer. Ceram. Soc.* January 1983, p. C31.
39. TRANTINA, G. *J. Amer. Ceram. Soc.* v. 62, no. 7-8, 1979, p. 377.
40. GOVILA, R. *Ceramic Life Prediction Parameters.* U.S. Army Materials Technology Laboratory, MTL TR 80-18, May 1980.
41. GOVILA, R. *J. Amer. Ceram. Soc.* v. 65, no. 1, 1982, p. 15.
42. TIGHE, N., and WEIDERHORN, S. *Fracture Mechanics of Ceramics.* v. 6, p. 403.
43. BRATTON, R., and MILLER, D. Ceramics for High Performance Applications, II. J. Burke, E. Lenoe, and R. Katz, ed., Brook Hill Publ. Co., Chestnut Hill, Mass., 1978, p. 689.
44. MILLER D., ANDERSON, C., SINGHAL, S., LANGE, F., DIAZ, E., KOSSOWSKY, R., and BRATTON, R. *Brittle Materials Design, High Temperature Gas Turbine Material Technology, Final Report.* U.S. Army Materials and Mechanics Research Center, CTR 76-32, v. 4, December 1976.
45. LANGE, F. F. *Int. Met. Rev.* no. 1, 1980, p. 1.
46. TIGHE, N. J. *J. Mat. Sci.* v. 13, 1978, p. 1455.
47. KOSSOWSKY, R., MILLER, D., and DIAZ, E. *J. Mat. Sci.* v. 10, 1975, p. 983.
48. TIGHE, N. J., WIEDERHORN, S. M., CHUANG, T. J., and McDANIEL, C. L. in Deformation in Ceramic Materials II. R. Tressler and R. Bradt, ed., Plenum Press, New York, 1984, p. 587.
49. JAKUS, K., RITTER, J. R., Jr., and FAHEY, J. P. *Comm. Amer. Ceram. Soc.* September 1982, C143.

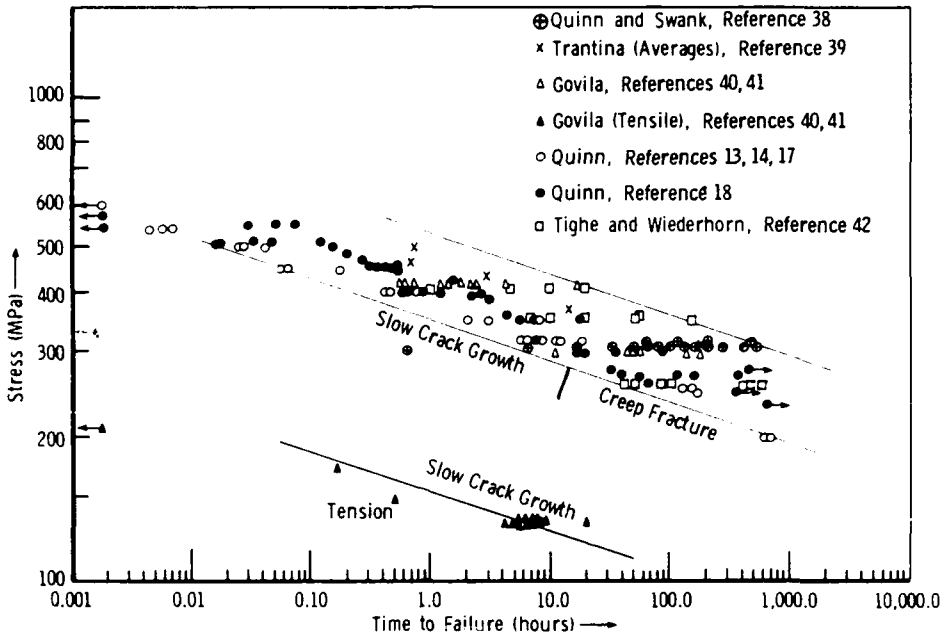

Figure 4. Stress rupture results for HPSN at 1200°C. There is a remarkable consistency in the flexural results. Elastic flexure stresses are shown. The tension results are shifted to lower stresses.

Figure 5 is an alternative representation of the same stress rupture data. In this instance, the graph has axes of stress and temperature and the loci are for constant failure times. These loci were interpolated from graphs, such as Figure 3. The reason for presenting the data in this format will be evident shortly.

Figure 6 shows the results for 162 specimens with the artificially implanted, 50-micron-deep flaws. The fast fracture strength is 370 MPa and is marked with a bar. Each labelled point in the figure corresponds to a stress temperature condition at which stress rupture experiments were conducted. The points are labelled by a ratio which gives the number of specimens that did fail from the artificial flaw to the total number tested. The number in parentheses is the geometric mean time-to-failure. For example, at 266 MPa and 1200°C, of seven specimens tested, six broke at the flaw and the geometric mean time-to-failure was 60 hours.

Figure 7 shows fracture surfaces with obvious SCG from the artificial flaw. The intergranular SCG zone, relative to the transgranular artificial flaw and subsequent fast fracture zones, makes fractographic interpretation quite easy, which is another reason why this material is suitable as a model ceramic. Severe oxidation and surface pitting can occur during the experiments, as shown in Figure 7b. This undoubtedly reduces the strength, yet this degradation mechanism never did "catch up" with the SCG or creep fracture mechanisms.*

Note that four experiments of extreme duration are of special interest. Three experiments were performed at 1100°C and 266 MPa. Only two specimens were tested to failure, one at 17,376 and one at 14,941 hours (see Figure 6). These failed in the gage length and not at the load pins. The former broke from the artificial flaw but with 1.9% strain. The latter failed such that the fracture surface had several tiers, including one with the artificial

*There is one instance where a surface pit did cause a time-dependent failure. This was a tension specimen tested by Govila[40,41] at 1204°C at 133 MPa which failed at the atypical time of 21 hours. This probably was due to an excessive surface oxide reaction due to contaminants from strain gage burn-off.

flaw on it, probably by coincidence. This specimen certainly failed due to creep fracture and had a final strain of 1.7%. The third experiment was regrettably terminated at 10,000 hours while the specimen was still intact due to an equipment problem. The final extreme duration experiment was performed at 1150°C and 200 MPa with failure occurring at 9,100 hours, but not from the artificial flaw.

Figure 8 shows a specimen that failed from creep fracture. Tighe[46] showed similar extreme creep cracking. Creep fracture is typically more severe at the surface,[47] presumably due to the lower constraint relative to an internal crack. Similarly, edge creep cracking will often be more severe, as shown in Figure 8.

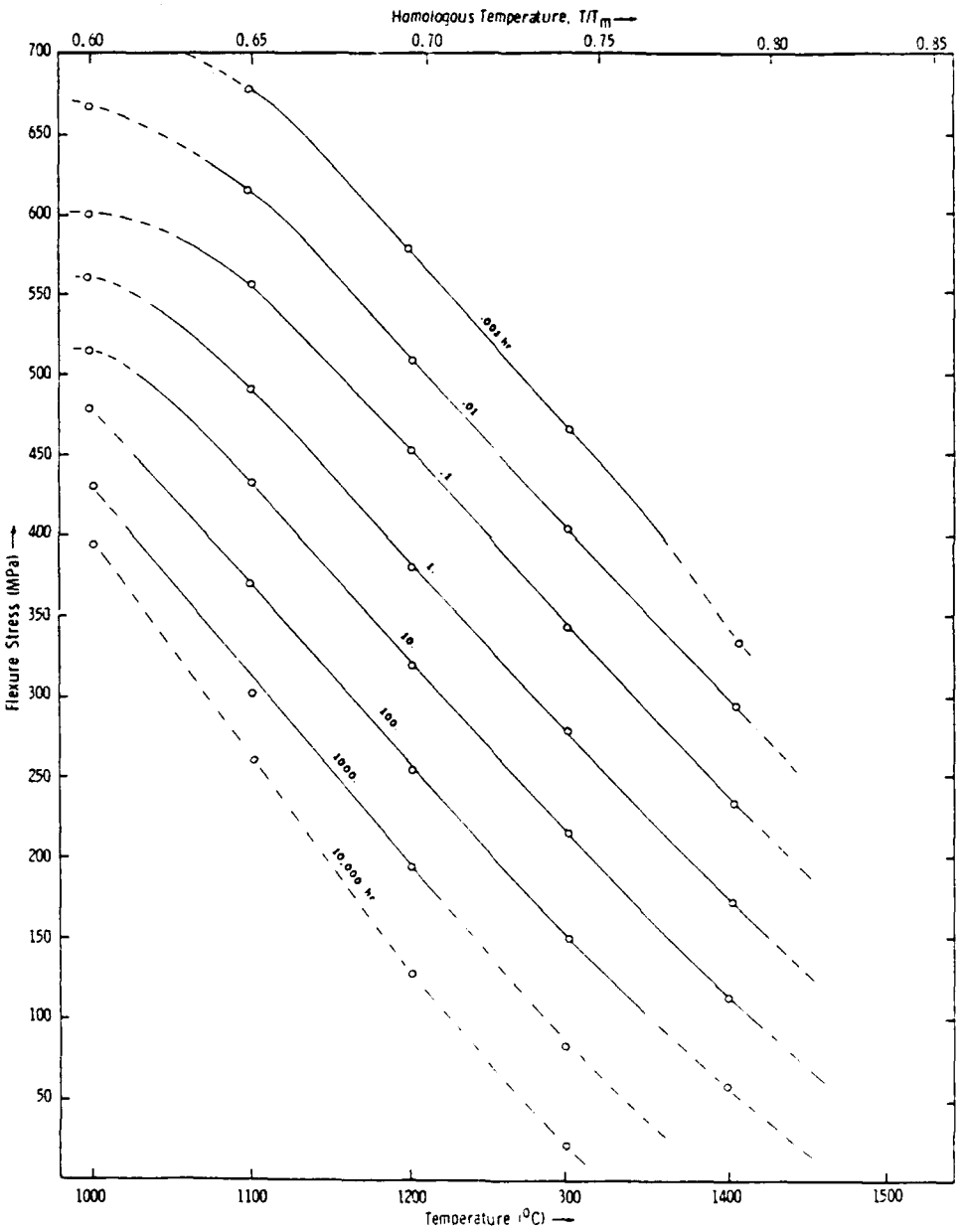

Figure 5. Flexural stress rupture results for as-machined HPSN specimens. This is an alternative representation of the results of Figure 3. The loci are constant failure time in hours.

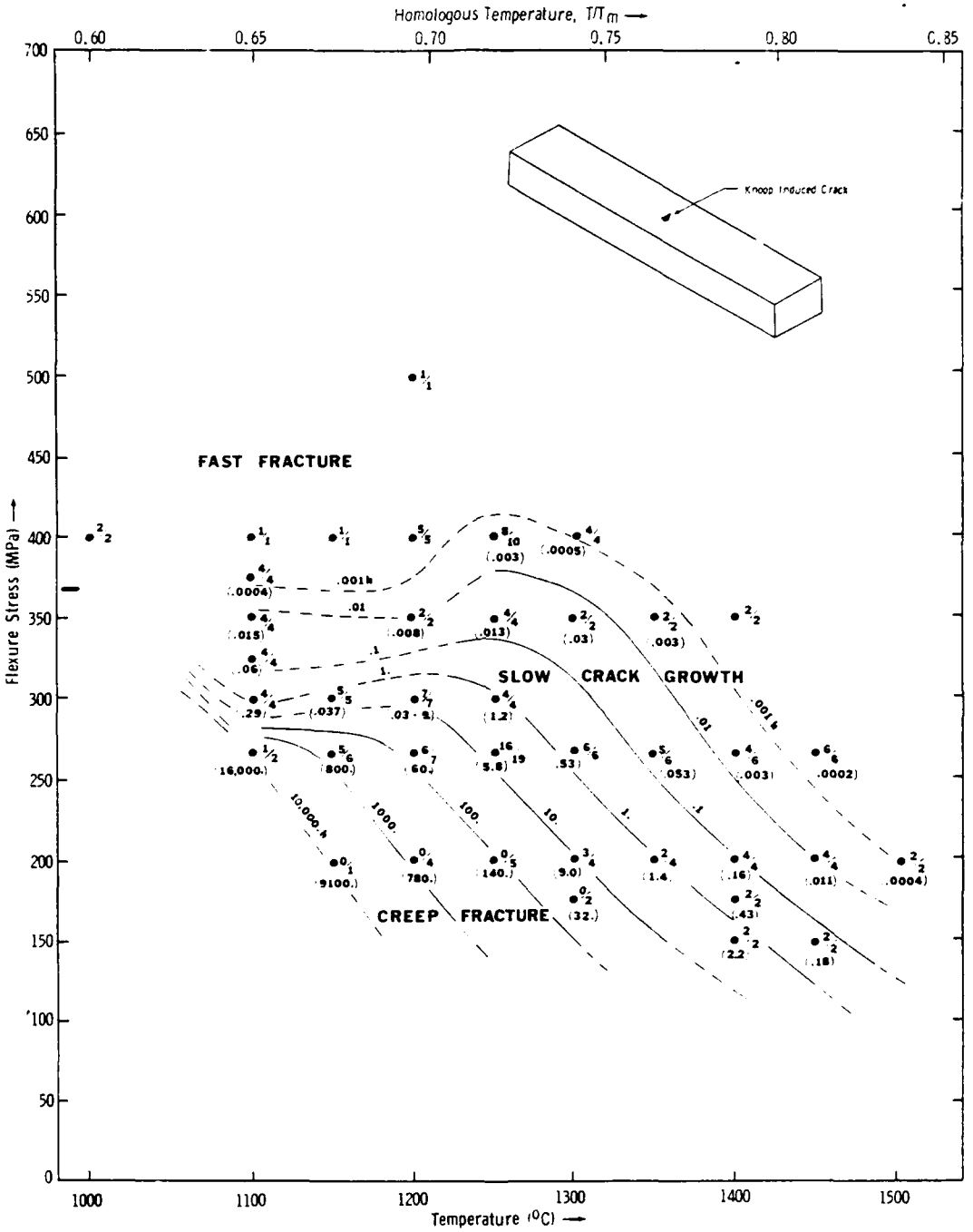

Figure 6. Flexural stress rupture results for artificially-flawed HPSN specimens. Each dot is a stress-temperature combination where experiments were performed. The dot is labelled by a ratio which gives the number of specimens that broke from the artificial flaw relative to the total number of specimens tested. The geometric mean time-to-failure is given in parentheses. Loci of constant failure time in hours are shown. In the creep fracture regime, none of the specimens failed from the artificial flaw.

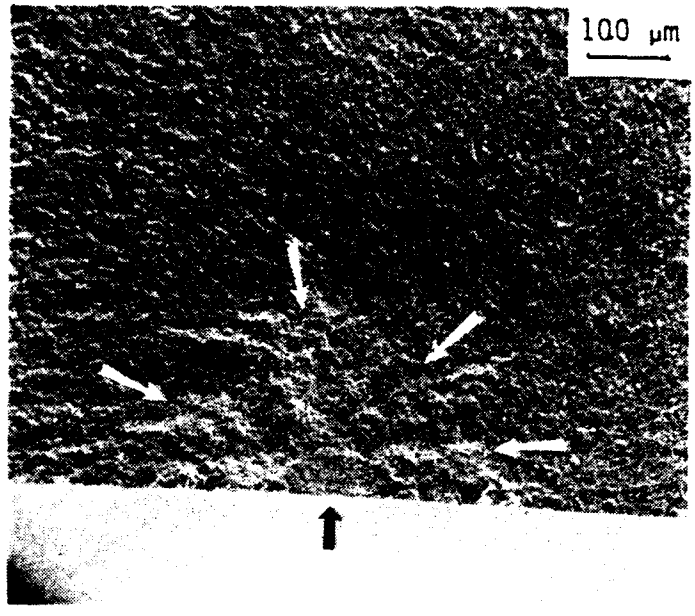

(a)

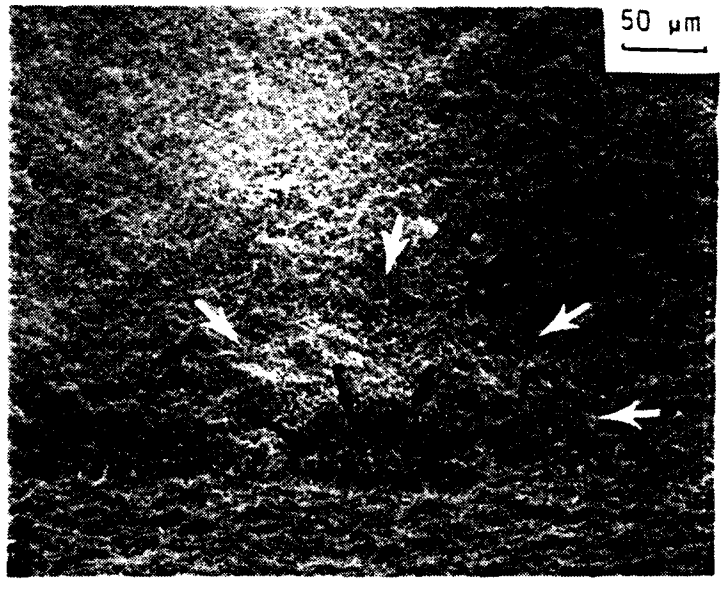

(b)

Figure 7. HPSN fracture surfaces illustrating SCG (white arrows) from the Knoop defect (black arrows). (a) was loaded to 400 MPa at 1250°C and failed at 10 seconds. (b) was loaded at 175 MPa at 1300°C. The test was interrupted at 210 hours and the specimen broken at room temperature. Surface oxidation is much more severe than in (a).

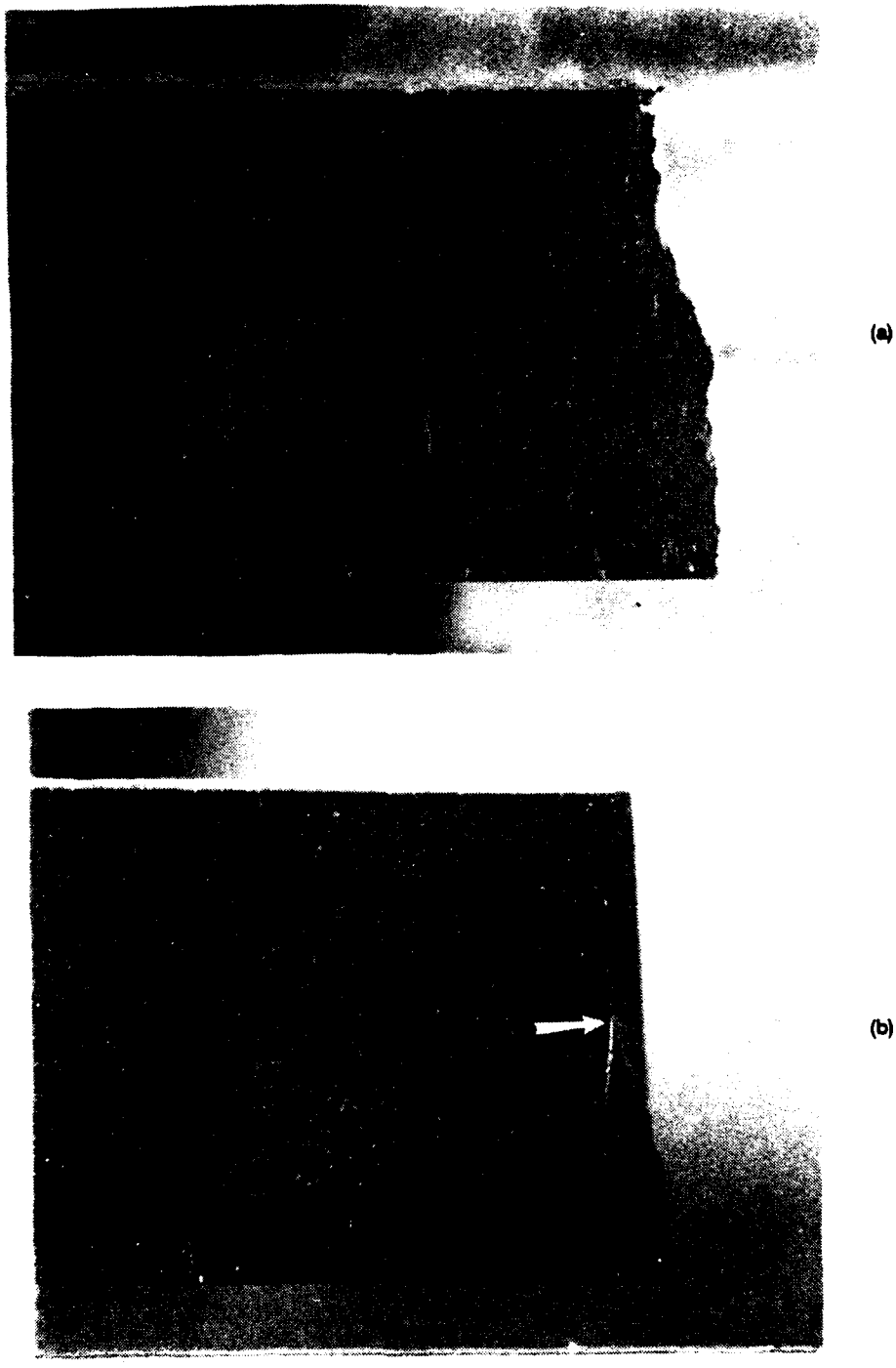

Figure 8. Extreme microcracking on the tensile surface of HPSN specimens that failed in creep fracture. The fracture surface is to the right. (a) shows a specimen that failed after 1157 hours at 1200°C with 200 MPa. The specimen did not fail from the artificial flaw. (b) shows a specimen which failed after 14,491 hours at 1100°C at 266 MPa. The arrow notes the location of the original artificial flaw.

In one instance where a large number of experiments (19) were performed at the same condition (266 MPa, 1250°C), the log of time-to-failure was normally distributed. The geometric mean and the median, therefore, coincide. The geometric mean was 5.7 hours and the standard deviation was 0.13.

DISCUSSION

Over much of the field in Figure 6, failure did occur as the result of SCG from the artificial flaws. Alternatively, at lower stresses, there is a distinct regime where creep fracture was dominant, since creep deformation was significant and specimens **did not** fail from the dominant original flaws. Instead, fracture was controlled by creep fracture. Excessive creep plasticity blunted the initial defects, restricting their growth. Ultimately, however, the high deformation leads to extensive microcrack nucleation, growth, interaction, and, finally, rupture. One of the principle findings of this work is that fractographic analysis is capable of discerning the conditions wherein either slow crack growth or alternatively creep fracture mechanisms are dominant.

Das et al.[28] have supportative findings in that five flexure specimens at 1300°C and 196 MPa did not break from 2.6 kg Knoop flaws implanted in them. This is not surprising since the conditions are close to the creep fracture regime in Figure 6. Times-to-failure were appreciably shorter than in the present study, but the latter study was in vacuum. Kossowsky et al.[47] clearly show the substantial decrease in stress rupture lifetime and strain in inert atmospheres relative to air for HPSN.

The SCG versus creep fracture regimes are further defined by comparing the loci of failure time of the artificially-flawed versus the as-machined specimens, as shown in Figure 9. Over much of the field, slow crack growth from preexisting flaws did lead to fracture. The artificially-flawed specimens (solid lines) failed in less time than similarly loaded as-machined specimens (dotted lines) since there was less crack growth necessary to reach a critical condition. In sharp contrast, however, the failure loci coincide under some conditions, which means the artificial flaws **had no effect whatsoever** upon the failure time. This is the creep fracture regime.

Total apparent strains in the creep fracture regime were of the order of one percent or more and there was no clear correlation of the creep fracture-SCG boundary with percent deformation, as shown in Figure 10. The apparent strain is an underestimate, however, since the neutral axis migrates into what once was the compression half of the specimen.[31]

The shaded boundary, which separates the SCG and creep fracture regimes, levels off at about 260 MPa. This level is influenced by the size of the initial artificial flaws.[14] The larger the initial flaws, the more likely SCG will cause fracture, and the boundary can be shifted somewhat.

The apparent activation energies for the two mechanisms can be assessed in Figure 11. Artificially-flawed specimens loaded at 200 MPa or 266 MPa encompass both the creep fracture and SCG regimes. There is no significant change in slope in either line, implying the same activation energy applies to both mechanisms. The apparent energies are 211 and 216 kcal/gmole, which is in reasonable agreement with the 180 kcal/gmole estimated from the **natural** flaw experiments (see Equation 3). This is the activation energy for a

grain boundary sliding process involving the viscous grain boundary phase which accounts for **both** SCG and creep. Transmission electron microscopy studies of HPSN stress rupture specimens have confirmed that this mechanism is responsible for creep deformation, creep fracture, and slow crack growth.[46-48,50] Mosher et al.[51] reported an activation energy for viscous flow of the grain boundary phase of 166 kcal/gmole in HS 130, which is a similar grade HPSN.* Ud Din and Nicholson[50] found an activation energy of 140 kcal/gmole for flexure specimens tested in creep loading. Kossowsky et al.[47] performed direct tension experiments on the same earlier grade HPSN and reported 130 to 150 kcal/gmole but noted that the activation energy increased with increasing purity of the boundary phase. They further noted that lifetime was limited by the creep rate (clearly indicating a creep rupture mode of failure), which is not surprising since their stresses were only 30 MPa to 110 MPa. Nevertheless, they also observed conditions where crack growth from preexisting flaws (in the SCG regime) led to shorter lifetimes than from creep fracture. Seltzer[52] reported 168 kcal/gmole for both the HS 130 and NC 132 grades of HPSN. However, Arons and Tien[25] noted two activation energies: 202 kcal/gmole for the persistent component of creep and 172 kcal/gmole for the viscoelastic component.

In summary, the SCG versus creep fracture regimes could be defined by two methods: a comparison of times-to-failure between artificial and naturally-flawed specimens and by fractographic observations (Does a large initial flaw grow to failure?). Reference 14 further interprets certain aspects of these results, including the effects of residual stresses, atmospheric effects, preoxidation effects, and the influence of initial flaw size upon the map boundaries.

Figure 12 puts the results into perspective since the entire range of stress-temperature conditions are shown. The fast fracture strength at room temperature is modelled by Weibull statistics.[53,54] The median (50%) and 10% and 90% confidence intervals are shown. A gradual weakening of the material occurs to about 900°C,[40,43,44] but the strength limiting flaws are probably the same if the tests are done in the fast fracture mode. However, flaw healing or new flaw generation can alter the fast fracture strength, as shown, even for relatively short exposure times.[55] The onset of static fatigue phenomena occurs in the 800°C to 900°C range in air, but scatter is high. Above 1000°C, slow crack growth from preexisting flaws becomes increasingly consistent and it is possible to mark loci of median failure time. Figure 12 shows the median line (50%) for fast fracture strength splits into loci of median failure time. The creep fracture regime is put into its proper perspective in Figure 12 where it is shown as a small field at high temperature and low stress. Finally, in the flexural mode of loading, excessive creep causes specimens to not fracture, but bottom out on the test fixtures. This is shown in Figure 12 as "Deformation Limited". Such a field is not expected for the tensile mode of loading unless superplasticity occurs, but this has not been reported as yet for this material. The failure controlling or life prediction parameters for each field are given in Table 1.

*HS 130 grade, Norton Company, Worcester, Mass. and Joseph Lucas Company, West Midlands, U.K. Torti[15] explains the minor difference between HS 130 and NC 132 grades of HPSN.

50. UD DIN, S., and NICHOLSON, P. *J. Mat. Sci.* v. 10, 1975, p. 1375.
51. MOSHER, D. R., RAJ, R., and KOSSOWSKY, R. *J. Mat. Sci.* v. 11, 1976, p. 49.
52. SELTZER, M. *Amer. Ceram. Soc. Bul.* v. 56, no. 4, 1977, p. 418.
53. WEIBULL, W. *J. Appl. Mech.* v. 18, 1951, p. 293.
54. DAVIES, D. G. S. *Proc. Br. Ceram. Soc.* v. 22, 1973, p. 429.
55. TIGHE, N. J., and WIEDERHORN, S. M. Fracture Mechanics of Ceramics. R. Bradt, A. Evans, D. Hasselman, and F. Lange, ed.,

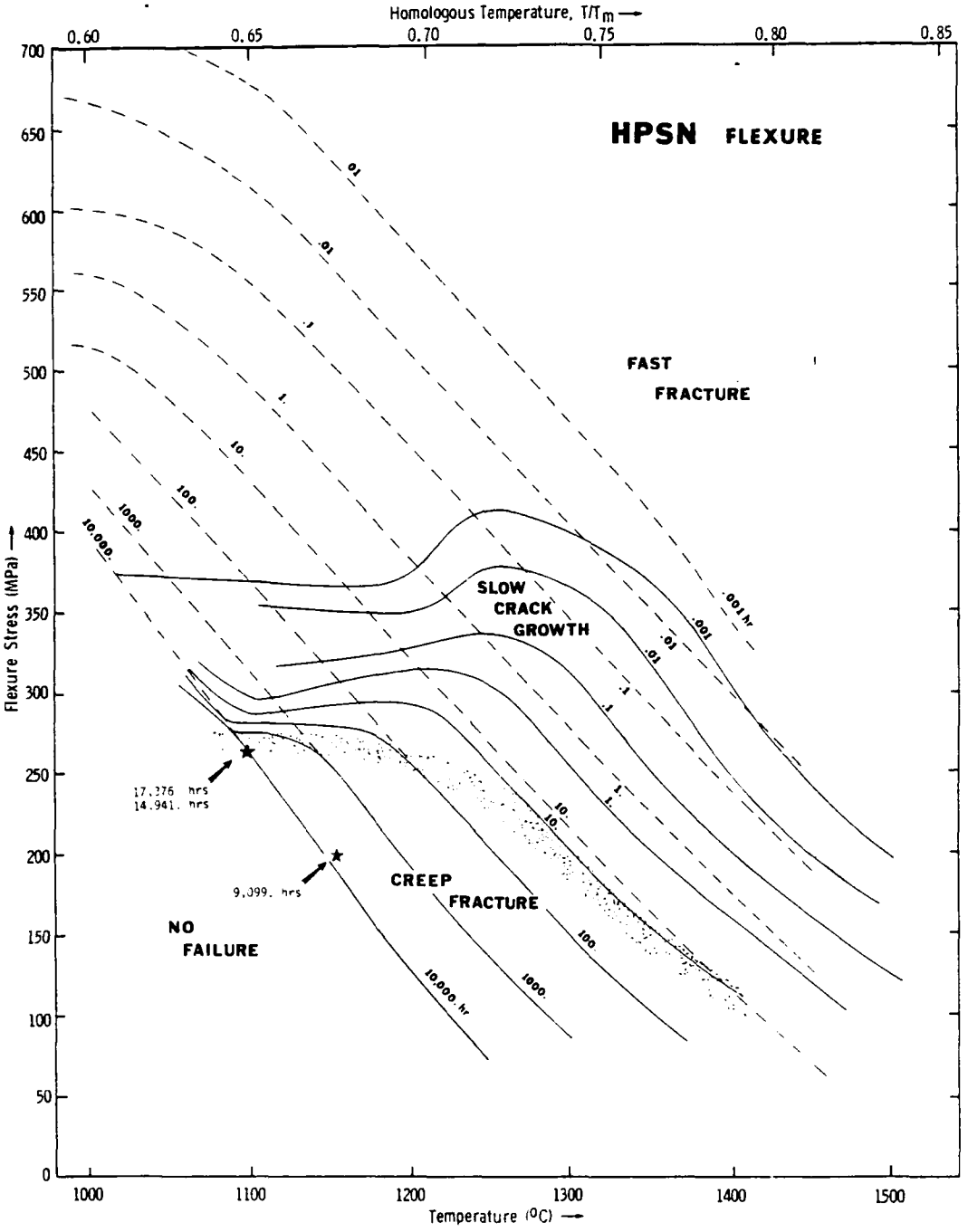

Figure 9. Combined natural (dotted) and artificial (solid) flaw, HPSN stress rupture data. The coincidence of the loci of failure time for both specimen types determines the creep fracture regime. All stresses are elastic flexure stresses. The stars highlight three unusually long experiments. The stars highlight three unusually long experiments.

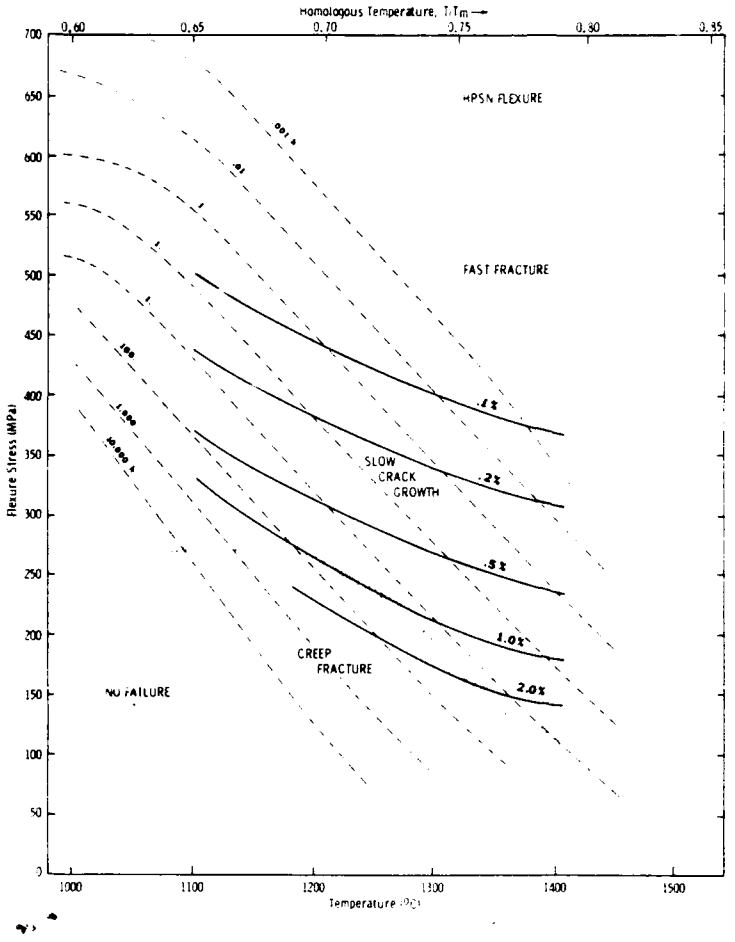

Figure 10. Apparent final creep strains superimposed on the HPSN fracture map.

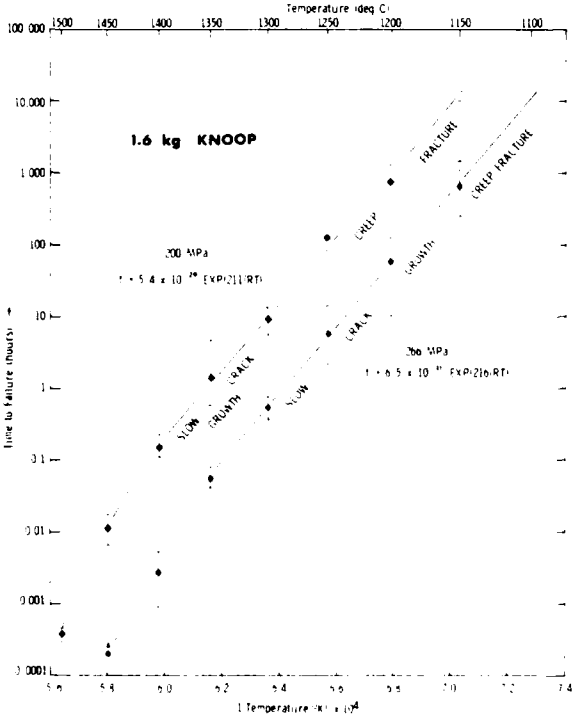

Figure 11. Activation energies for creep fracture and a slow crack growth are the same in HPSN.

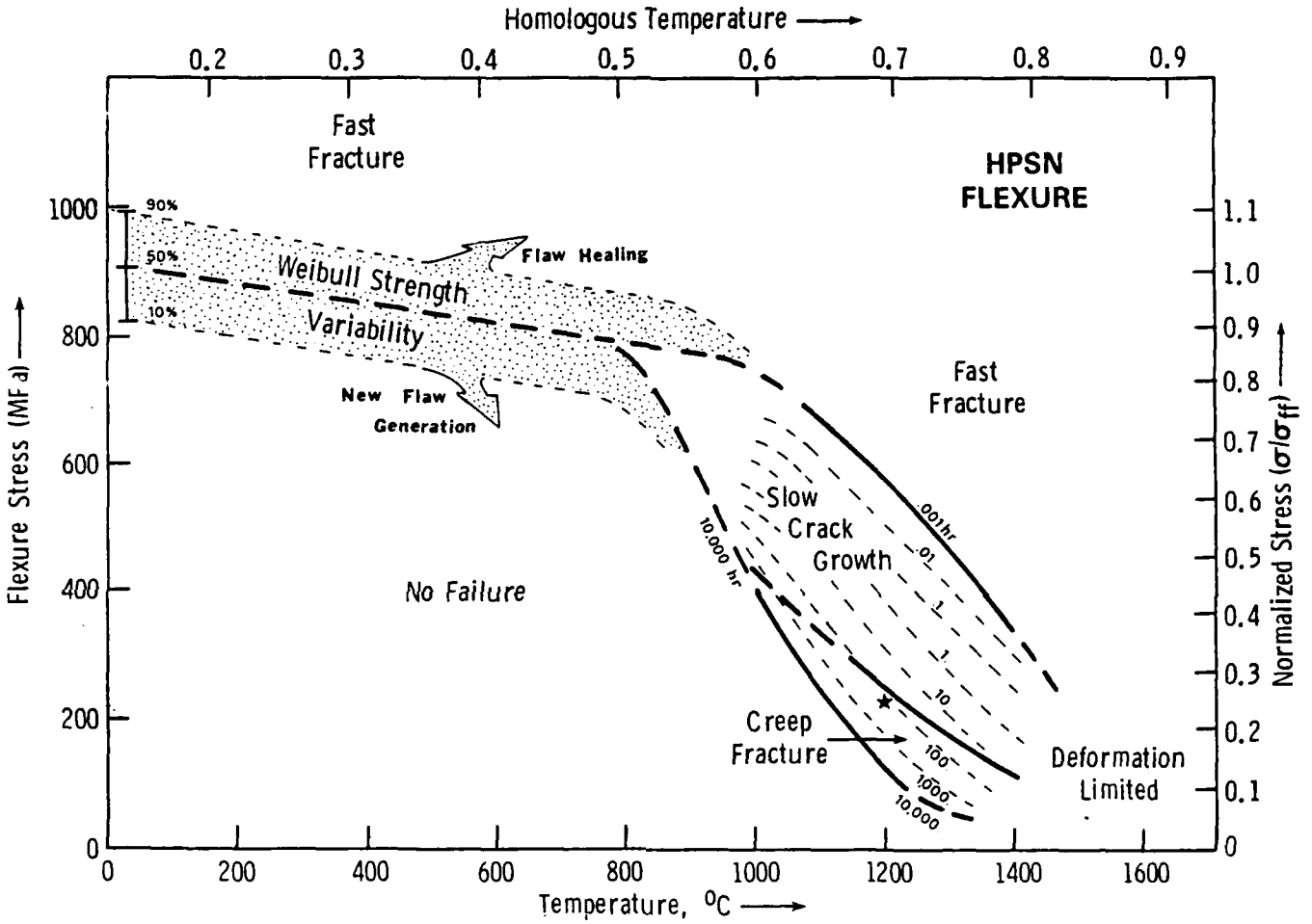

Figure 12. Comprehensive fracture map for MgO-doped HPSN tested in flexure in air. The star corresponds to the conditions used by Tighe and Wiederhorn[56] for their strength degradation maps.

Table 1. PARAMETERS CONTROLLING THE STRENGTH AND LIFE PREDICTION OF HPSN

Field	Controlling Factors	References	HPSN Grade NC 132‡
No Failure	Stress is too low to cause fracture. Specimens remain intact. For all flaws present, the stress intensity is sufficiently low, i.e.:		K_{Ic} = 4.5 to 5.0 (Ref. 17) $^{MN/m^{1.5}}$
	$K_I < K_{Ic}$ where:		
	$K_I = Y \sigma_a c^{1/2}$ Where Y is a shape factor, σ_a is the applied stress, c is the flaw size		
	Specimens can retain same strength, weaken, or strengthen somewhat, due to flaw healing, blunting, or generation of new flaws.	Tighe and Wiederhorn[55]	
Fast Fracture	Stress is too high and causes brittle fracture. For one or more flaws, the stress intensity is too high: $K_I > K_{Ic}$		
Boundary Between Fast Fracture and No Failure	Boundary is actually a field due to statistical aspects of the strength of ceramics. Failure is a probabilistic event. Weibull statistics applicable:		
	Probability of Fracture $P = 1 - \exp -\int^{V} \left(\frac{\sigma_\alpha - \sigma_u}{\sigma_o}\right)^{\frac{1}{m}} dV$	Weibull[53] Davies[54]	
	Where m is the Weibull modulus, σ_u is the threshhold stress, σ_o is a normalization parameter called the characteristic strength, V is the specimen volume		m = 17.2 σ_u = 0 σ_o = 988 MPa for a 1.0 mm^3 effective volume
	Note: Uniaxial loading with a single flaw population assumed. The integration can be over the surface if surface flaws predominate.		
Slow Crack Growth	Fracture due to slow crack growth of preexisting flaws. Crack velocity (v) is related to the applied stress intensity:		
	$v = A K_I^N \exp(-Q_{scg}/RT)$	Evans et al.[35] Charles[34]	Q_{scg} = 180 - 210 kcal/gmole
	Where Q_{scg} is the activation energy, T is the temperature, N is the slow crack growth exponent, A is a constant		N at 1000°C = 30 1100°C = 19.5 1200°C = 12.8 1300°C = 9.9 1400°C = 9.2
	For constant applied stress (stress rupture loading): the crack velocity can be integrated to give the time to failure (t_f):	Davidge et al.[36] Ritter et al.[37]	(N values for this HPSN are surveyed in Ref. 17)
	$t_f = \sigma_a^{-N} c_i^{(2-N/2)} \exp(Q_{scg}/RT)$		c_i = 18-30 μm (Ref. 15)
	Where c_i is the initial flaw size		(An alternative expression is given by Eq. 3)
Creep Fracture	Fracture is due to the accumulation of excessive creep deformation and damage. This may entail the nucleation, growth, and coalescence of microcracks. Given steady state creep where:		
	$\dot{\varepsilon}_{ss} = B \sigma_a^n \exp(-Q_c/RT)$		
	Where $\dot{\varepsilon}_{ss}$ is the steady state strain rate, Q_c is the activation energy for creep, B,n are constants		
	$t_f \dot{\varepsilon}_{ss}^{m^*} = C$	Monkman Grant[56] Johnson et al.[3]	m^* = 1.0 C = 2.9×10^{-2} for t_f in hours (Ref. 47, HS 130 grade of HPSN
	Where m^* and C are constants		

‡All parameters were evaluated in the present study, unless otherwise stated.

56. MONKMAN, F. C., and GRANT, N. J. Proc. ASTM 56, 1956, p. 593.

Deformation maps are well known, but fracture maps are relatively recent. Gandhi and Ashby[10] presented a preliminary diagram for the HS 130 vintage HPSN. Their terminology for the SCG regime was "brittle intergranular fracture 3." They used normalized temperature and stress axes. The temperature axis was homologous temperature, which is the absolute temperature normalized by the melting temperature. In the present report, T_m is set at the decomposition temperature of silicon nitride, which is 1850°C.[45] Figures 5, 9, 10, and 12 of this report include such a normalized axis.* Gandhi and Ashby normalized their stress axis by the elastic modulus, but this ignores differences such as flexure versus tension testing and artificial versus natural flaws. The fast fracture stress is preferred as a normalization parameter since it takes these factors into consideration.

Grathwohl and his colleagues have also noted the different regimes of slow crack growth and creep fracture in a magnesia-doped HPSN at 1200°C and 1300°C.[21,57-59] Their work included detailed flexural creep strain and oxidation measurements. The transition from SCG to creep fracture was 180 MPa at 1200°C and 150 MPa at 1300°C in as-machined specimens. These stress levels are similar to those shown in Figures 9 and 12. Grathwohl showed a distinct time lag when the mechanism of failure shifted. (Such time lag was not observed in the HPSN of the present study.) The time lag and the pattern of the applied stress versus time-to-failure plots were directly accounted for by stress relaxation in flexure.[21,59] Grathwohl further noted that specimens did not fail from artificial flaws in the creep fracture regime, but that very large artificial flaws (multiple 10 kg Knoop indents) tended to extend the creep fracture-SCG boundary to lower stress values, enhancing the SCG regime.[59] Grathwohl's findings and interpretations of the multiple mechanisms of static fatigue failure are in complete accord and are a fascinating complement to the present report.

The fracture map, as shown in Figure 12, is for flexure specimens under constant loading in air. Alternative loading sequences, or preoxidizing treatments, can have significant affect upon strengths and lifetimes. Oxidation of magnesia-doped HPSN can influence stress rupture performance by creating surface damage or by altering the composition of the second phase at the silicon nitride grain boundaries. This can be either from preoxidation treatments or by oxidation concurrent with a stress rupture experiment. Quinn and Swank[38] showed that a 100 hour preexposure in air at 1200°C radically decreased static fatigue lifetimes due to the formation of large surface pits from which SCG occurred during subsequent stress rupture testing. This is in contrast to reports of the beneficial effects of such a preexposure due to the formation of a surface sink of silica that draws cation impurities or the Mg additive to the surface, thereby improving the refractoriness of the grain boundary phase in the bulk.[27,60,61] In each of these latter instances, however, it was necessary to remove the oxide layer from the specimen to gain the benefit. The effect of prior exposure upon the fast fracture strength is also considerable.[38,55,62]

Oxidation of MgO-doped HPSN during the stress rupture experiment can lead to increased creep rates[47,52] and times-to-failure[47,52,58] relative to experiments in inert

*The homologous temperature axes, in previous References 12, 13, 14, and 16 were in error.

57. GRATHWOHL, G. *Int. J. High Tech. Ceram.* v. 4, no. 2, 1988, p. 123.
58. ERNSTBERGER, U., GRATHWOHL, G., and THUMMLER, F. Ceramic Materials and Components for Engines. W. Bunk and H. Hausner, ed., Deutsche Keramische Gesselschaft, Berlin, Germany, 1986, p. 485.
59. GRATHWOHL, G. Creep and Fracture of Engineering Materials and Structures. B. Wilshire and D. Owen, ed., Pineridge Press, Swansea, United Kingdom, 1984, p. 565.
60. LANGE, F. F., and DAVIS, B. I. *Bul. Amer. Ceram. Soc.* v. 59, 1980, p. 827.
61. LANGE, F. F., DAVIS, B. I., and METCALF, M. G. *J. Mat. Sci.* v. 18, 1983, p. 1497.
62. JAKUS, K., RITTER, J., Jr., and ROGERS, W. P. *J. Amer. Ceram. Soc.* v. 67, no. 7, 1984, p. 471.

atmosphere. Grathwohl[59] showed that the oxide layer formed is not oxidation rate limiting in Mg-doped HPSN, and that the creep and slow crack growth resistance of a specimen has a gradient due to the outward diffusion of Mg to the surface oxide sink. An activation energy of 120 kcal/gmole was measured for this process. Lange et al.[61] have demonstrated this compositional gradient. It, therefore, appears there is an interrelationship between oxidation and the grain boundary sliding processes that result in creep and slow crack growth phenomena. This can unfortunately complicate life prediction analysis. For example, there could be a creep or lifetime dependence upon specimen size, related to the diffusion distance for cations to reach the surface. In laboratory flexure specimens, these distances are not significantly different,* but real components may be 10 times thicker.

Multiaxial loadings which might be expected to drastically change the stress rupture lifetimes have, in fact, not been particularly deleterious in MgO-doped HPSN, providing the reduced fast fracture strength in multiaxial loading is taken into account.[63,64]

COMPARISON OF TENSION TO FLEXURE RESULTS

The utility of the fracture map would be greatly enhanced if it could be generalized to modes of loading other than flexure. It is, therefore, useful to compare the available tensile stress rupture data to flexure data. Govila[40,41] performed tensile stress rupture tests on this same grade HPSN at 1000°C, 1204°C, and 1300°C. Figures 4, 13, and 14 show the results in comparison to flexure data of the present study. The tension results at 1000°C are highly scattered, making comparison difficult. At 1200°C and 1300°C, the direct tension results are shifted to lower stresses, which is not surprising in light of the Weibull size effect of strength, and the relaxations in stress to be expected in flexure tests. What is encouraging is the shifts seem to be by a simple proportional amount in the 0.1 to 100 hour range, and this suggests steady state phenomena.† Table 2 gives these proportional shifts. It was possible from reexamining the detailed fractographs, shown by Govila,[40] to assess the mechanism of failure in his tensile specimens, and these are noted in Figures 4, 13, and 14. There was only slow crack growth (usually from internal sources) and no creep fracture at 1000°C and 1200°C. At 1300°C, the fracture surfaces were slow crack growth for specimens loaded higher than 80 MPa, but at lower stresses crack growth zones were huge (> 50% of the fracture surface) and jagged corresponding to the onset of creep fracture. Thus, there seem to be grounds for assuming the mechanisms of time-dependent failure are the same for the flexure and tension experiments, a fortuitous result.

Table 2. RATIO OF FLEXURE TO TENSILE STRENGTH AT CONSTANT FAILURE TIME FOR HPSN

	1000°C	1200°C	1300°C
1 Hour	1.7	2.7	2.7
10 Hours	1.6	2.6	2.8

*Unpublished work by E. M. Lenoe at MTL demonstrated there may be a size effect upon lifetime in laboratory flexure specimens.

†The lines through the flexure data were least square curve fitted, whereas the lines through the tension data were handdrawn.

63. QUINN, G., and WIRTH, G. Ceramic Materials and Components for Engines. V. Tennery, ed., Amer. Ceram. Soc., Westerville, Ohio, 1984, p. 874.

64. QUINN, G., and WIRTH, G. *Mat. Sci. and Eng.* v. A109, 1989, p. 147.

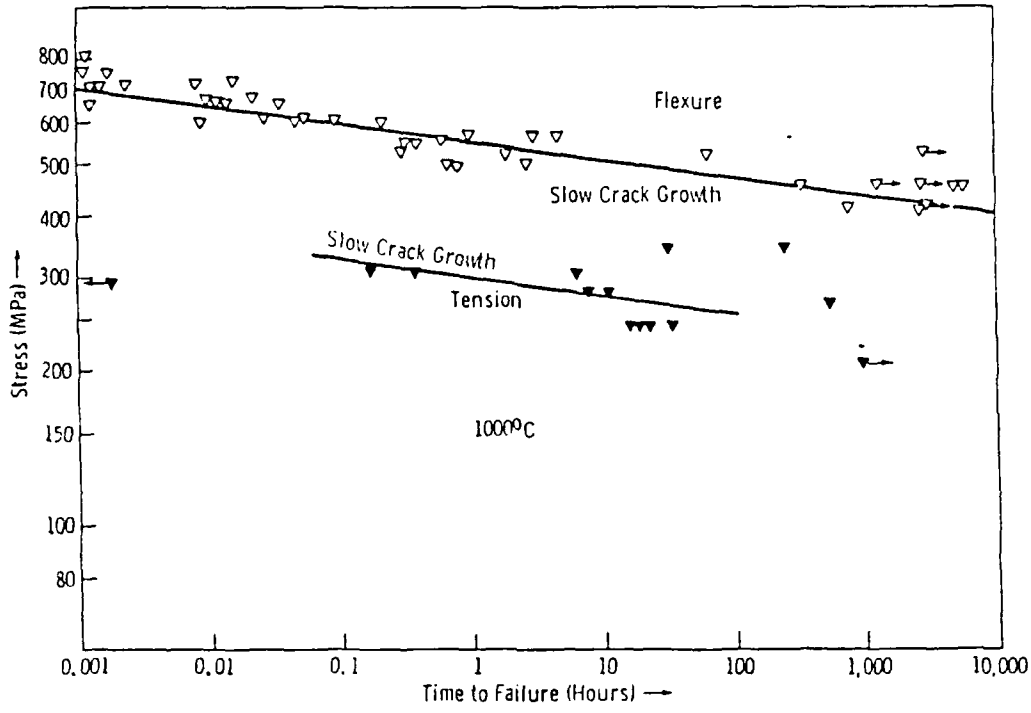

Figure 13. Tensile[40,41] and flexural (this report) stress rupture data for HPSN at 1000°C in air.

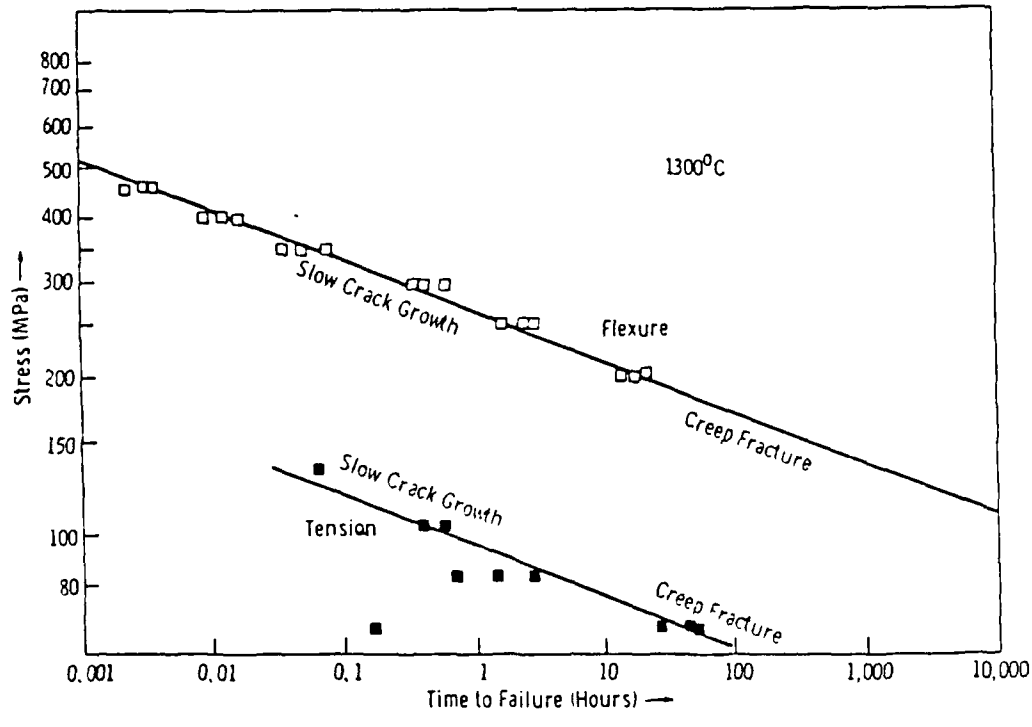

Figure 14. Tensile[40,41] and flexural (this report) stress rupture data for HPSN in air.

The dependence of strength upon specimens size is well known and well modelled by Weibull statistics. Davies[54] shows that strength can be correlated between different specimen sizes and modes of loading through the effective volumes (V_E):

$$\frac{\sigma_{flex.}}{\sigma_{tens.}} = \left(\frac{V_{E,tens.}}{V_{E,flex.}}\right)^{\frac{1}{m}} \tag{4}$$

The effective volume of Govila's tension specimens is approximately equal to the volume in the gage length and was 154 mm^3. The effective volume of the flexure specimens is:

$$V_{E,flex.} = V\,[(m + 2) / 4\,(m + 1)^2] \tag{5}$$

which ranged from 3.3 mm^3 to 4.8 mm^3 for the flexure specimens used in this study. The equation then suggests the ratio of flexure strength to tension strength is 1.2 to 1.3. This, coincidentally, is in good agreement with the ratio of 1.35 reported by Ohji[65] for HPSN at room and 1200°C for a different HPSN tested both in tension and flexure. The present ratio is somewhat less than the estimated 1.6 to 1.7 experimental ratio observed at 1000°C for specimens with failure times greater than 0.1 hour (see Table 2). The difference could easily be accounted for by the onset of limited creep relaxation in the flexure specimens, differences in the specimen preparation of billet sources, or any one of the assumptions in the Weibull size analysis.* One significant experimental error with the flexure specimens is the friction constraint due to fixed points of loading.[66] The friction error is well known in room temperature fixtures and typically causes stresses in the specimens to be reduced by 5% to 15% from what is computed from simple beam theory.[66] Very little has been reported at elevated temperatures, but preliminary experiments at the U.S. Army Materials Technology Laboratory (MTL) with the same HPSN used in this study indicate the error is of the order of 10 percent for stress rupture specimens at 1200°C over all times from loading to 100 hours. Thus, the stress correction for flexure to tensile stress becomes 1.3 x 1.1 = 1.4, which is in better agreement with the observed results.

Relaxation of the tensile stresses will occur in flexure specimens at temperatures where creep occurs. The great difficulty of properly interpreting flexural creep data has been discussed previously. For the present purposes, consider the steady state phenomena (in the 1 to 100 hour range in which much of the primary creep has diminished) and use the conventional constitutive equation:

$$\dot{\varepsilon}_{ss} = B\,\sigma_a^n \exp\,(-Q_c/RT) \tag{6}$$

where $\dot{\varepsilon}_{ss}$ is the steady state creep rate, B and n are constants, and Q_c is the activation energy for creep. This relationship has been shown to be suitable with a stress exponent n of 2.0 by a number of investigators.[25,45,47,67,68] An important and necessary adjustment to this constitutive relationship is to note creep rates in tension are appreciably higher than those in

*A two parameter Weibull function is assumed with volume flaws. The same class flaws are assumed to be responsible for failure in each specimen type. It is often difficult to determine the original natural flaw origin when significant slow crack growth has occurred. The pertinent flaws to compare at the high temperature flexure stress rupture conditions could very well be volume flaws, as proven in Reference 17. Govila[40,41] showed very convincingly that the tension SCG origins at 1000°C and 1200°C were internal.

65. OHJI, T. *Int. J. High Tech. Ceram.* v. 4, no. 2, 1988, p. 211.
66. BARATTA, F. I., QUINN, G. D., and MATTHEWS, W. T. *Errors Associated With Flexure Testing of Brittle Materials.* U.S. Army Materials Technology Laboratory, MTL TR 87-35, July 1987.
67. HOLLENBERG, G. W., TERWILLIGER, G. R., and GORDON, R. S. *J. Amer. Ceram. Soc.* v. 54, 1971, p. 196.
68. TALTY, P. K., and DIRKS, R. A. *J. Mat. Sci.* v. 13, 1978, p. 580.

compression for the same stress and temperature. Fortunately, Seltzer[52] has shown that for this HPSN the activation energy and stress exponents are the same in tension and compression, and the difference in creep rates is a simple proportionality constant. While many authors have cited ratios of tension to compression creep rates for HPSN in the literature (for example, References 20 and 24), there appears to be only three specific original experiments to actually measure the phenomena, as shown in Table 3. Talty and Dirks[68] used trapezoidal-shaped flexure specimens to intentionally measure the different creep rates. Seltzer[52] combined data from several sources, including his own tensile and compression work, and got ratios of 4.7 or 9.3, depending upon whether HS 130 or NC 132 data was used. The exact ratio is a consequence of the grain boundary phase composition and chemistry, as noted by Lange.[45] It is especially interesting to observe Seltzer's work was over a broad temperature range, 1200°C to 1400°C. Kossowsky et al.[47] mention a **single** experiment at 1370°C where 689 MPa compressive stress was required to achieve the same creep rate for a tensile specimen at 69 MPa. This compression to tension stress ratio of 10 can be converted to an equivalent creep rate of 100 times faster in tension than compression if the stress exponent is 2. This is only one experiment (albeit a much cited one) and it is felt that the compressive specimen probably was loaded in a stress regime wherein there may have been a higher creep exponent (4+), as shown in References 25 and 47. Thus, it seems reasonable to rely upon the results of the more comprehensive former studies and use:

$$\dot{\varepsilon}_t = (5 \text{ to } 9) \times \dot{\varepsilon}_c \, . \tag{7}$$

Table 3. RATIO OF TENSILE TO COMPRESSIVE CREEP RATES IN HPSN

	Method	Temperatures-Stresses	Ratio
Talty and Dirks[68]	Tapered Flexure Specimens	1250°C - 1300°C 66 MPa - 156 MPa	5.6
Seltzer[52]	Tension and Compression	1200°C - 1400°C 68 NPa	4.7 - 9.3
Kossowsky, Miller and Diaz[47]	Tension and Compression	1370°C 68 MPa	100

Two analyses have been done for the case of steady state creep, modelled by Equation 6, with different constants B for tension and compression.[20,23] (Grathwohl's analysis[20] is in terms of S, the ratio of compressive to tension stresses to get the same creep rates. The ratios of creep rates cited above can readily be converted to an S factor by noting the stress exponent n is 2 in Equation 6.) The stress for steady state conditions in the flexure specimen is reduced by a factor of 1.5 or 1.6, depending upon whether a creep rate ratio of 5 or 9 is used. Thus, in summary, combining the correction factors for adjusting flexure to tension:

$$\sigma_f = (1.3) \times (1.1) \times (1.5 \text{ to } 1.6) \times \sigma_t = 2.1 \text{ to } 2.3 \, \sigma_t \tag{8}$$

which, although not in complete agreement with the experimentally observed shifts of 2.6 to 2.8, is qualitatively correct.

Figure 15 is a fracture map for direct **tension** loading for this grade HPSN. The overall form and the fields are in accordance with the flexure fracture map (see Figure 12), but available tension data from the literature were used to set the stress and temperature values.[40,41,43,44,47] The homologous temperature axis has been extended to 0 and the inert strength is assumed to be the same as the fast fracture strength at room temperature, since no

known static fatigue phenomena are active at these low temperatures. The band separating the fast fracture and no failure zones at low temperature is again depicted by a shaded zone with 10%, 50%, and 90% Weibull confidence limits. A shallow trend of diminishing strength is shown, as reported previously.[40,43,44] The median fast fracture line then splits into median lines of constant failure time in the zone where slow crack growth becomes operative (T > 900°C). The loci of failure time are empirical results from the work of Govila.[40,41] These lines have much less certainty than the flexure loci, since the tension results had much higher scatter. Govila, unfortunately, did not report fast fracture or inert tension strength results to compliment his superb stress rupture data. An inert strength can be estimated from extrapolating his 1000°C tension stress rupture results back to 0.001 hours (see Figure 13) at the same slope as the flexure results. (Creep deformation in the flexure data is negligible at this temperature[25] and the elastic flexure stresses are probably not relaxed.) This estimated tension fast fracture strength, at 1000°C, is then adjusted by the amount of strength degradation that occurs from room to 1000°C, which is approximately 11% from References 40, 43, and 44 and the flexure results of this study. Thus, the fast fracture room temperature tension strength is estimated to be 500 MPa. Of course, this should be evaluated for each batch of material and each given specimen size since Weibull size effects will influence this value.

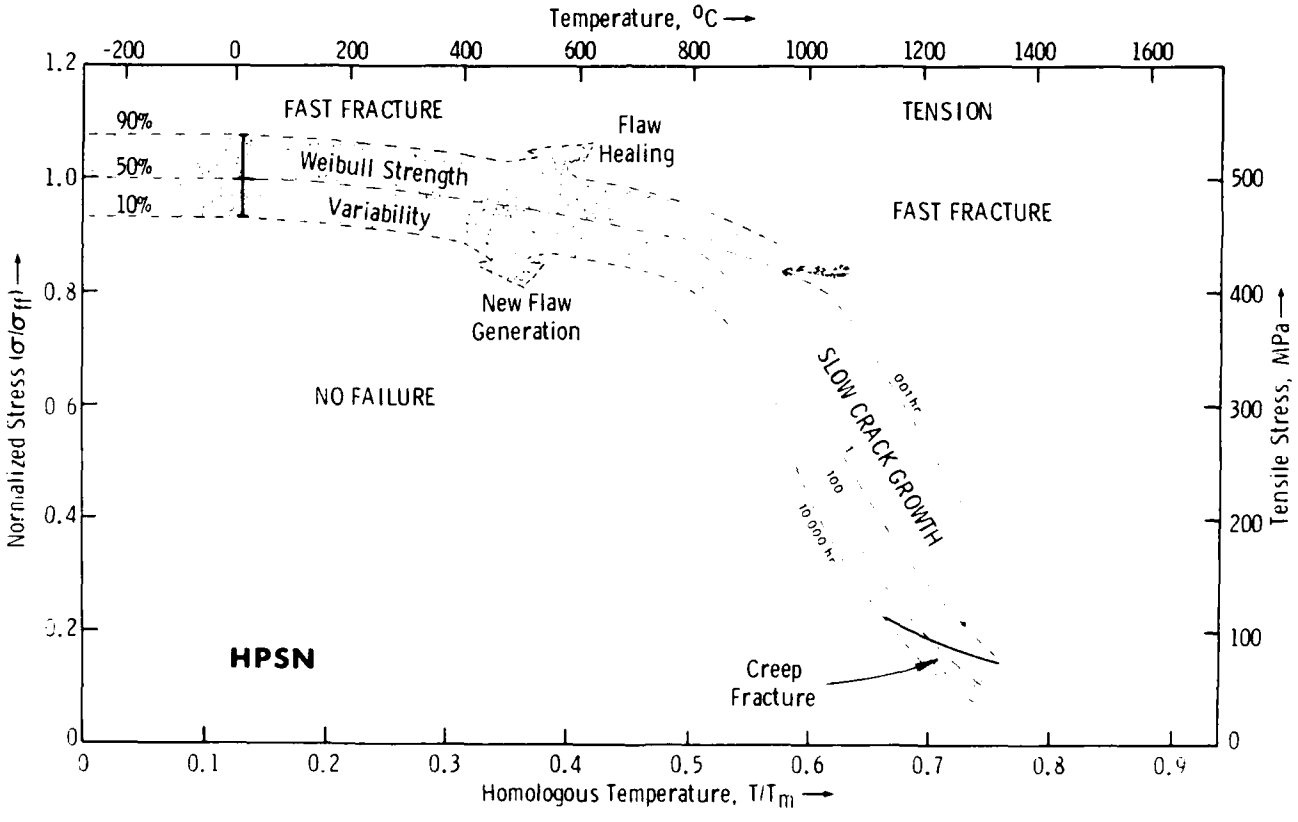

Figure 15. Fracture map for MgO-doped HPSN in air in direct tension.

The fracture maps (see Figures 12 and 15) integrate and reconcile the static fatigue results of all previous MgO-doped HPSN studies. Batch-to-batch material variations lead to fast fracture variability of about 20%, and times-to-failure vary by a factor of 10, but otherwise results are in excellent agreement. The comprehensive tension creep and stress rupture data of Kossowsky et al.[47] on the HS 130 grade was primarily in the low stress, high temperature creep fracture field. Their work conclusively demonstrated that a Monkman-Grant relationship (see Table 1) describes lifetime over a wide temperature range (1150°C to 1315°C) with failure times from 20 to 1920 hours. The more recent tension work by Govila on NC 132 was at higher stresses and primarily caused slow crack growth failures.

The strength degradation map of Tighe and Wiederhorn[55] would correspond to one single point on the flexure fracture map (see Figure 12) at 250 MPa and 1200°C. Their map shows a detailed evolution of retained fast fracture strength, for stress rupture specimens loaded at that **one** condition. Over one hundred flexure specimens were loaded at this condition. At regular intervals, several were broken to determine the fast fracture strength. After an initial strengthening, due to healing of machining damage, strength began to degrade due to the creation of new defects (pits on the surface). Ultimately, creep cavitation occurred leading to fracture at times over 500 hours, with a median failure time of about 1500 hours. The fracture maps of this study (see Figures 9 and 12) show creep fracture is indeed the cause of fracture, but with failure times about 200 hours, a difference most likely due to material variability.

An alternative procedure of stress rupture testing, interrupted static fatigue, has been advocated by Minford and Tressler[69] for silicon carbide, and later by Foley and Tressler[70] for sintered silicon nitride. Stress rupture specimens are loaded at a variety of stresses and temperatures. At the same elapsed time (10 or 100 hours), all experiments are stopped and the fast fracture strength is measured. It is possible to determine a stress corrosion *limit* (or threshold stress intensity factor) below which no time dependent failure will occur. The method was not applied to a MgO-doped HPSN, but, in principle, it would define the lower boundary between the "no failure" and "creep fracture" or "slow crack growth" regimes on the fracture maps.

The latter studies raise the issue of whether the more fundamental driving force for fracture is stress or stress intensity. Which should be used as the vertical axis on the fracture maps? As shown in Table 1, stress intensity does control both fast fracture and slow crack growth. Determination of stress intensity in a loaded component is difficult, however, due to uncertainties in the flaws and, particularly, their severity (the factor Y in Table 1). Stress intensity is irrelevant in the creep fracture regime and stress is the more fundamental parameter. Johnson et al.[3] have similarly noted the shortcomings of the use of stress intensity for materials under creep fracture conditions. Thus, it would seem that stress is an adequate parameter to characterize the driving force for fracture. Its usage on ceramic fracture maps will make the maps consistent with the deformation and fracture maps already in use for metallic and polymeric materials.

Although, in principle, the fracture mechanism map can be theoretically derived, it was empirically developed in the present study. The slow crack growth and creep fracture regimes are identifiable by comparison of times-to-failure of artificially-flawed versus as-machined

69. MINFORD, E. J., and TRESSLER, R. E. *J. Amer. Ceram. Soc.* v. 66, no. 5, 1983, p. 338.
70. FOLEY, M. R., and TRESSLER, R. E. *Adv. Ceram. Mat.* v. 3, no. 4, 1981, p. 382.

specimens. This approach must be used with extreme caution on other materials, however, since it can strongly bias results towards slow crack growth as the mechanism of failure. For example, it was shown in a stress rupture study on sintered silicon carbide that the use of artificially-flawed specimens **completely masked** the presence of a stress corrosion phenomenon involving surface connected porosity.[71] Johnson et al.[3] also reported that artificial flaws grew differently than natural defects in an alumina. Fractography is a key tool for fracture map development. Other studies have noted that changes in slope on stress rupture graphs[11,58] or changes in creep strains to fracture[58] can distinguish different regimes of static fatigue failure.

Fracture maps are probably better derived from stress rupture experiments rather than fracture mechanics tests. The latter have been disappointing in many instances (especially at high temperature, and particularly with HPSN) in their ability to correlate to stress rupture data on lab specimens[17,72,73] or components.*,[74] Large crack, fracture mechanics test results are irrelevant in many instances, such as for predicting creep fracture or surface stress corrosion attack of residual pores or microporous zones in advanced ceramics.

How much testing is necessary to devise a fracture map? This will depend upon the material. Over 500 flexure specimens were needed to create the comprehensive HPSN maps. This is partially a consequence of the statistical nature of strength of ceramics. Several dozen complimentary tension results were critical in extending the utility of the map to more generalized loading. Future stress rupture studies should feature judicious and complimentary flexure and tension stress rupture experimentation. A companion paper[11] develops a fracture map for a more contemporary sintered silicon nitride but with far fewer specimens.

CONCLUSIONS

The fracture map combines all of the mechanisms that limit the strength of a ceramic and puts them into perspective. Two mechanisms of static fatigue at elevated temperature exist in HPSN: creep fracture and slow crack growth. Both are related to the deformation of the intergranular second phase. The difference is a matter of scale. Creep deformations in the slow crack growth regime are confined to the immediate vicinity of a crack tip and lead to crack extension. Bulk deformation will alternatively lead to creep fracture. Several empirical approaches were used to develop the fracture maps. Fracture mechanism maps can be appreciated by and can guide the work of both the engineering and materials science communities.

*Reference 73 is one of the few successful instances.

71. QUINN, G. D., and KATZ, R. N. *J. Amer. Ceram. Soc.* v. 63, no. 1-2, 1980, p. 117.
72. PLETKA, B., and WEIDERHORN, S. *J. Mat. Sci.* v. 22, 1987, p. 1247.
73. QUINN, G. D. *J. Mat. Sci.* v. 22, 1987, p. 2309.
74. BAKER, R. R., SWANK, L. R., and CAVERLY, J. C. *Ceramic Life Prediction Methodology - Hot Spin Disc Life Program.* U.S. Army Materials and Mechanics Research Center, TR 83-44, August 1983.

REFERENCES

1. QUINN, G. D. *Ceram. Eng. Sci. Proc.* v. 3, no. 1-2, 1982, p. 77.
2. WIEDERHORN, S. M., HOCKEY, B. J., KRAUSE, R. F., and JAKUS, K. *J. Mat. Sci.* v. 21, 1986, p. 810.
3. JOHNSON, S. M., DALGLEISH, B. J., and EVANS, A. G. *J. Am. Ceram. Soc.* v. 67, 1984, p. 759.
4. BLUEMENTHAL, W., and EVANS, A. G. *J. Am. Ceram. Soc.* idem, p. 751.
5. OKADA, T., and SINES, G. *J. Amer. Ceram. Soc.* v. 66, no. 10, 1983, p. 719.
6. ROBERTSON, A. G., and WILKINSON, D. S. Fracture Mechanics of Ceramics. R. C. Bradt, A. G. Evans, D. P. H. Hasselman, and F. Lange, ed., Plenum Press, New York, v. 7, 1986, p. 311.
7. HASSELMAN, D. P. H., VENKATESWAREN, A., and SHIH, C. *Surfaces and Interfaces in Ceramic and Ceramic Metal Systems.* Materials Science Research, J. Pask, and E. Evans, ed., Plenum Press, New York, v. 14, 1981, p. 323.
8. WRAY, P. J. *J. Appl. Phys.* v. 40, 1969, p. 4018.
9. FIELDS, R. J., WEERASOORIYA, T., and ASHBY, M. F. *Met. Trans. A.* v. 11A, 1980, p. 333.
10. GANDHI, C., and ASHBY, M. *Acta Met.* v. 27, 1979, p. 1565.
11. QUINN, G. D., and BRAUE, W. R. Submitted to J. Mat. Sci., 1990.
12. QUINN, G. D *Methods for Assessing the Structural Reliability of Brittle Materials.* S. W. Freiman and C. M. Hudson, ed., American Society of Testing and Materials, Philadelphia, Pennsylvania, ASTM STP 844, 1984, p. 177.
13. QUINN, G. D. *Ceram. Eng. Sci. Proc.* v. 5, no. 7-8, 1984, p. 596.
14. QUINN, G. D. Fracture Mechanics of Ceramics. R. Bradt, A. Evans, D. Hasselman, and F. Lange, ed., Plenum Press, New York, v. 8, 1986, p. 319.
15. TORTI, M. L. Ceramics for High Performance Applications III, Reliability. E. Lenoe, R. Katz, and J. Burke, ed., Plenum Press, New York, 1983, p. 261.
16. QUINN, G. D. Ceramic Materials and Components for Engines. W. Bunk and H. Hausner, ed., Deutsche Keramische Gesselschaft, Berlin, Germany, 1986, p. 931.
17. QUINN, G. D., and QUINN, J. B. Fracture Mechanics of Ceramics. R. Bradt, A. G. Evans, D. Hasselman, and F. Lange, ed., Plenum Press, New York, v. 6, 1983, p. 603.
18. QUINN, G. D. *Characterization of Turbine Ceramics After Long-Term Environmental Exposure.* U.S. Army Materials Technology Laboratory, AMMRC TR 80-15, 1980.
19. QUINN, G. D. *Guide to the Construction of A Simple 1500°C Test Furnace.* U.S. Army Materials Technology Laboratory, AMMRC TN 77-4, August 1977, republished as TR 83-1, January 1983.
20. COHRT, H., GRATHWOHL, G., and THUMMLER, F. *Res. Mech. Let.* v. 1, 1981, p. 159.
21. GRATHWOHL, G. Deformation of Ceramic Materials, II. R. Tressler and R. Bradt, ed., Plenum Press, New York, 1984, p. 573.
22. FETT, T. *J. Mat. Sci. Let.* v. 6, 1987, p. 967.
23. FETT, T., and MUNZ, D. *Int. J. High Tech. Ceram.* v. 4, 1988, p. 281.
24. FETT, T., KELLER, K., and MUNZ, D. *J. Mat. Sci*, v. 23, 1988, p. 467.
25. ARONS, R., and TIEN, J. *J. Mat. Sci.* v. 15, 1980, p. 2046.
26. CARROLL, D. F., CHUANG, T. J., and WIEDERHORN, S. M. *Ceram. Eng. Soc. Proc.* v. 9, no. 7-8, 1988, p. 635.
27. WILKINSON, D. S. *J. Amer. Ceram.* Soc. v. 71, 1988, p. 562.
28. DAS, G., MENDIRATTA, M. G., and CORNISH, G. R. *J. Mat. Sci.* v. 17, 1982, p. 2486.
29. GRATHWOHL, G., and THUMMLER, F. *J. Mat. Sci.* v. 13, 1978, p. 1177.
30. VENKATESWAREN, A., and HASSELMAN, D. P. H. *J. Mat. Sci.* v. 16, 1981, p. 1627.
31. ROSENFIELD, A. R., DUCKWORTH, W. H., and SHETTY, D. K. *J. Amer. Ceram. Soc.* v. 68, 1985, p. 485.
32. JAKUS, K., and WIEDERHORN, S. *J. Amer. Ceram. Soc.* v. 71, no. 10, 1988, p. 832.
33. WIEDERHORN, S., CHUCK, L., FULLER, E., and TIGHE, N. *Tailoring of Multiphase and Composite Ceramics.* Materials Science Research, R. E. Tressler, G. L. Mecholsky, C. G. Pantano, and R. E. Newnham, ed., Plenum Press, New York, v. 20, 1986, p. 755.
34. CHARLES, R. J. *J. Appl. Phys.* v. 29, no. 12, 1958, p. 1657.
35. EVANS, A. G., RUSSELL, L. R., and RICHERSON, D. W. *Met. Trans. A.* v. 6A, 1975, p. 707.
36. DAVIDGE, R., McLAREN, J., and TAPPIN, G. *J. Mat. Sci.* v. 8, 1973, p. 1699.
37. RITTER, J., Jr. Fracture Mechanics of Ceramics. R. Bradt, D. Hasselman, and F. Lange, ed., Plenum Press, New York, v. 4, 1978, p. 667.
38. QUINN, G. D., and SWANK, L. *Comm. Amer. Ceram. Soc.* January 1983, p. C31.
39. TRANTINA, G. *J. Amer. Ceram. Soc.* v. 62, no. 7-8, 1979, p. 377.
40. GOVILA, R. *Ceramic Life Prediction Parameters.* U.S. Army Materials Technology Laboratory, MTL TR 80-18, May 1980.
41. GOVILA, R. *J. Amer. Ceram. Soc.* v. 65, no. 1, 1982, p. 15.
42. TIGHE, N., and WEIDERHORN, S. *Fracture Mechanics of Ceramics.* v. 6, p. 403.
43. BRATTON, R., and MILLER, D. Ceramics for High Performance Applications, II. J. Burke, E. Lenoe, and R. Katz, ed., Brook Hill Publ. Co., Chestnut Hill, Mass., 1978, p. 689.
44. MILLER D., ANDERSON, C., SINGHAL, S., LANGE, F., DIAZ, E., KOSSOWSKY, R., and BRATTON, R. *Brittle Materials Design, High Temperature Gas Turbine Material Technology, Final Report.* U.S. Army Materials and Mechanics Research Center, CTR 76-32, v. 4, December 1976.
45. LANGE, F. F. *Int. Met. Rev.* no. 1, 1980, p. 1.
46. TIGHE, N. J. *J. Mat. Sci.* v. 13, 1978, p. 1455.
47. KOSSOWSKY, R., MILLER, D., and DIAZ, E. *J. Mat. Sci.* v. 10, 1975, p. 983.
48. TIGHE, N. J., WIEDERHORN, S. M., CHUANG, T. J., and McDANIEL, C. L. in Deformation in Ceramic Materials II. R. Tressler and R. Bradt, ed., Plenum Press, New York, 1984, p. 587.
49. JAKUS, K., RITTER, J. R., Jr., and FAHEY, J. P. *Comm. Amer. Ceram. Soc.* September 1982, C143.
50. UD DIN, S., and NICHOLSON, P. *J. Mat. Sci.* v. 10, 1975, p. 1375.
51. MOSHER, D. R., RAJ, R., and KOSSOWSKY, R. *J. Mat. Sci.* v. 11, 1976, p. 49.
52. SELTZER, M. *Amer. Ceram. Soc. Bul.* v. 56, no. 4, 1977, p. 418.
53. WEIBULL, W. *J. Appl. Mech.* v. 18, 1951, p. 293.
54. DAVIES, D. G. S. *Proc. Br. Ceram. Soc.* v. 22, 1973, p. 429.
55. TIGHE, N. J., and WIEDERHORN, S. M. Fracture Mechanics of Ceramics. R. Bradt, A. Evans, D. Hasselman, and F. Lange, ed., Plenum Press, New York, v. 5, 1983, p. 403.

56. MONKMAN, F. C., and GRANT, N. J. Proc. ASTM 56, 1956, p. 593.
57. GRATHWOHL, G. *Int. J. High Tech. Ceram.* v. 4, no. 2, 1988, p. 123.
58. ERNSTBERGER, U., GRATHWOHL, G., and THUMMLER, F. Ceramic Materials and Components for Engines. W. Bunk and H. Hausner, ed., Deutsche Keramische Gesselschaft, Berlin, Germany, 1986, p. 485.
59. GRATHWOHL, G. Creep and Fracture of Engineering Materials and Structures. B. Wilshire and D. Owen, ed., Pineridge Press, Swansea, United Kingdom, 1984, p. 565.
60. LANGE, F. F., and DAVIS, B. I. *Bul. Amer. Ceram. Soc.* v. 59, 1980, p. 827.
61. LANGE, F. F., DAVIS, B. I., and METCALF, M. G. *J. Mat. Sci.* v. 18, 1983, p. 1497.
62. JAKUS, K., RITTER, J., Jr., and ROGERS, W. P. *J. Amer. Ceram. Soc.* v. 67, no. 7, 1984, p. 471.
63. QUINN, G., and WIRTH, G. Ceramic Materials and Components for Engines. V. Tennery, ed., Amer. Ceram. Soc., Westerville, Ohio, 1989, p. 824.
64. QUINN, G., and WIRTH, G. *Mat. Sci. and Eng.* v. A109, 1989, p. 147.
65. OHJI, T. *Int. J. High Tech. Ceram.* v. 4, no. 2, 1988, p. 211.
66. BARATTA, F. I., QUINN, G. D., and MATTHEWS, W. T. *Errors Associated With Flexure Testing of Brittle Materials.* U.S. Army Materials Technology Laboratory, MTL TR 87-35, July 1987.
67. HOLLENBERG, G. W., TERWILLIGER, G. R., and GORDON, R. S. *J. Amer. Ceram. Soc.* v. 54, 1971, p. 196.
68. TALTY, P. K., and DIRKS, R. A. *J. Mat. Sci.* v. 13, 1978, p. 580.
69. MINFORD, E. J., and TRESSLER, R. E. *J. Amer. Ceram. Soc.* v. 66, no. 5, 1983, p. 338.
70. FOLEY, M. R., and TRESSLER, R. E. *Adv. Ceram. Mat.* v. 3, no. 4, 1981, p. 382.
71. QUINN, G. D., and KATZ, R. N. *J. Amer. Ceram. Soc.* v. 63, no. 1-2, 1980, p. 117.
72. PLETKA, B., and WEIDERHORN, S. *J. Mat. Sci.* v. 22, 1987, p. 1247.
73. QUINN, G. D. *J. Mat. Sci.* v. 22, 1987, p. 2309.
74. BAKER, R. R., SWANK, L. R., and CAVERLY, J. C. *Ceramic Life Prediction Methodology - Hot Spin Disc Life Program.* U.S. Army Materials and Mechanics Research Center, TR 83-44, August 1983.

DISTRIBUTION LIST

No. of Copies	To
1	Office of the Under Secretary of Defense for Research and Engineering, The Pentagon, Washington, DC 20301
	Commander, U.S. Army Laboratory Command, 2800 Powder Mill Road, Adelphi, MD 20783-1145
1	ATTN: AMSLC-IM-TL
1	AMSLC-CT
	Commander, Defense Technical Information Center, Cameron Station, Building 5, 5010 Duke Street, Alexandria, VA 22304-6145
2	ATTN: DTIC-FDAC
1	Metals and Ceramics Information Center, Battelle Columbus Laboratories, 505 King Avenue, Columbus, OH 43201
	Commander, Army Research Office, P.O. Box 12211, Research Triangle Park, NC 27709-2211
1	ATTN: Information Processing Office
	Commander, U.S. Army Materiel Command, 5001 Eisenhower Avenue, Alexandria, VA 22333
1	ATTN: AMCLD
	Commander, U.S. Army Materiel Systems Analysis Activity, Aberdeen Proving Ground, MD 21005
1	ATTN: AMXSY-MP, H. Cohen
	Commander, U.S. Army Missile Command, Redstone Scientific Information Center, Redstone Arsenal, AL 35898-5241
1	ATTN: AMSMI-RD-CS-R/Doc
1	AMSMI-RLM
	Commander, U.S. Army Armament, Munitions and Chemical Command, Dover, NJ 07801
2	ATTN: Technical Library
1	AMDAR-LCA, Mr. Harry E. Pebly, Jr., PLASTEC, Director
	Commander, U.S. Army Natick Research, Development and Engineering Center, Natick, MA 01760
1	ATTN: Technical Library
	Commander, U.S. Army Satellite Communications Agency, Fort Monmouth, NJ 07703
1	ATTN: Technical Document Center
	Commander, U.S. Army Tank-Automotive Command, Warren, MI 48397-5000
1	ATTN: AMSTA-ZSK
2	AMSTA-TSL, Technical Library
	Commander, White Sands Missile Range, NM 88002
1	ATTN: STEWS-WS-VT
	President, Airborne, Electronics and Special Warfare Board, Fort Bragg, NC 28307
1	ATTN: Library
	Director, U.S. Army Ballistic Research Laboratory, Aberdeen Proving Ground, MD 21005
1	ATTN: SLCBR-TSB-S (STINFO)
	Commander, Dugway Proving Ground, Dugway, UT 84022
1	ATTN: Technical Library, Technical Information Division
	Commander, Harry Diamond Laboratories, 2800 Powder Mill Road, Adelphi, MD 20783
1	ATTN: Technical Information Office
	Director, Benet Weapons Laboratory, LCWSL, USA AMCCOM, Watervliet, NY 12189
1	ATTN: AMSMC-LCB-TL
1	AMSMC-LCB-R
1	AMSMC-LCB-RM
1	AMSMC-LCB-RP
	Commander, U.S. Army Foreign Science and Technology Center, 220 7th Street, N.E., Charlottesville, VA 22901
1	ATTN: Military Tech

No. of Copies	To
	Commander, U.S. Army Aeromedical Research Unit, P.O. Box 577, Fort Rucker, AL 36360
1	ATTN: Technical Library
	Commander, U.S. Army Aviation Systems Command, Aviation Research and Technology Activity, Aviation Applied Technology Directorate, Fort Eustis, VA 23604-5577
1	ATTN: SAVDL-E-MOS
	U.S. Army Aviation Training Library, Fort Rucker, AL 36360
1	ATTN: Building 5906-5907
	Commander, U.S. Army Agency for Aviation Safety, Fort Rucker, AL 36362
1	ATTN: Technical Library
	Commander, USACDC Air Defense Agency, Fort Bliss, TX 79916
1	ATTN: Technical Library
	Commander, U.S. Army Engineer School, Fort Belvoir, VA 22060
1	ATTN: Library
	Commander, U.S. Army Engineer Waterways Experiment Station, P. O. Box 631, Vicksburg, MS 39180
1	ATTN: Research Center Library
	Commandant, U.S. Army Quartermaster School, Fort Lee, VA 23801
1	ATTN: Quartermaster School Library
	Naval Research Laboratory, Washington, DC 20375
1	ATTN: Code 5830
2	Dr. G. R. Yoder - Code 6384
	Chief of Naval Research, Arlington, VA 22217
1	ATTN: Code 471
1	Edward J. Morrissey, WRDC/MLTE, Wright-Patterson Air Force, Base, OH 45433-6523
	Commander, U.S. Air Force Wright Research & Development Center, Wright-Patterson Air Force Base, OH 45433-6523
1	ATTN: WRDC/MLC
1	WRDC/MLLP, M. Forney, Jr.
1	WRDC/MLBC, Mr. Stanley Schulman
	National Aeronautics and Space Administration, Marshall Space Flight Center, Huntsville, AL 35812
1	ATTN: R. J. Schwinghammer, EH01, Dir, M&P Lab
1	Mr. W. A. Wilson, EH41, Bldg. 4612
	U.S. Department of Commerce, National Institute of Standards and Technology, Gaithersburg, MD 20899
1	ATTN: Stephen M. Hsu, Chief, Ceramics Division, Institute for Materials Science and Engineering
1	Committee on Marine Structures, Marine Board, National Research Council, 2101 Constitution Ave., N.W., Washington, DC 20418
1	Librarian, Materials Sciences Corporation, Guynedd Plaza II, Bethlehem Pike, Spring House, PA 19477
1	The Charles Stark Draper Laboratory, 68 Albany Street, Cambridge, MA 02139
	Wyman-Gordon Company, Worcester, MA 01601
1	ATTN: Technical Library
	Lockheed-Georgia Company, 86 South Cobb Drive, Marietta, GA 30063
1	ATTN: Materials and Processes Engineering Dept. 71-11, Zone 54
	General Dynamics, Convair Aerospace Division, P.O. Box 748, Fort Worth, TX 76101
1	ATTN: Mfg. Engineering Technical Library
1	Mechanical Properties Data Center, Belfour Stulen Inc., 13917 W. Bay Shore Drive, Traverse City, MI 49684
	Director, U.S. Army Materials Technology Laboratory, Watertown, MA 02172-0001
2	ATTN: SLCMT-TML
1	Author

U.S. Army Materials Technology Laboratory
Watertown, Massachusetts 02172-0001
FRACTURE MECHANISM MAPS FOR ADVANCED STRUCTURAL CERAMICS. PART I: METHODOLOGY AND HOT-PRESSED SILICON NITRIDE RESULTS - George D. Quinn

Technical Report MTL TR 90-6, February 1990, 30 pp-illus-tables, D/A Project: 1L162105.AH84

AD____________
UNCLASSIFIED
UNLIMITED DISTRIBUTION

Key Words

Ceramics
Silicon nitride
Powders

The static fatigue behavior of advanced structural ceramics can be controlled by a variety of failure mechanisms. A fracture mechanism map can define the stress-temperature regimes where the different mechanisms are dominant. The static fatigue resistance of a hot-pressed silicon nitride with magnesia sintering aid is limited by slow crack growth or creep fracture, depending upon the specific stress-temperature conditions. The flexural fracture map is considerably refined relative to earlier versions, and in conjunction with available tension data, was used to create a tension fracture map. The fracture map brings together the findings of a number of studies and can be appreciated by materials scientists and engineers.

U.S. Army Materials Technology Laboratory
Watertown, Massachusetts 02172-0001
FRACTURE MECHANISM MAPS FOR ADVANCED STRUCTURAL CERAMICS. PART I: METHODOLOGY AND HOT-PRESSED SILICCN NITRIDE RESULTS - George D. Quinn

Technical Report MTL TR 90-6, February 1990, 30 pp-illus-tables, D/A Project: 1L162105.AH84

AD____________
UNCLASSIFIED
UNLIMITED DISTRIBUTION

Key Words

Ceramics
Silicon nitride
Powders

The static fatigue behavior of advanced structural ceramics can be controlled by a variety of failure mechanisms. A fracture mechanism map can define the stress-temperature regimes where the different mechanisms are dominant. The static fatigue resistance of a hot-pressed silicon nitride with magnesia sintering aid is limited by slow crack growth or creep fracture, depending upon the specific stress-temperature conditions. The flexural fracture map is considerably refined relative to earlier versions, and in conjunction with available tension data, was used to create a tension fracture map. The fracture map brings together the findings of a number of studies and can be appreciated by materials scientists and engineers.

U.S. Army Materials Technology Laboratory
Watertown, Massachusetts 02172-0001
FRACTURE MECHANISM MAPS FOR ADVANCED STRUCTURAL CERAMICS. PART I: METHODOLOGY AND HOT-PRESSED SILICON NITRIDE RESULTS - George D. Quinn

Technical Report MTL TR 90-6, February 1990, 30 pp-illus-tables, D/A Project: 1L162105.AH84

AD____________
UNCLASSIFIED
UNLIMITED DISTRIBUTION

Key Words

Ceramics
Silicon nitride
Powders

The static fatigue behavior of advanced structural ceramics can be controlled by a variety of failure mechanisms. A fracture mechanism map can define the stress-temperature regimes where the different mechanisms are dominant. The static fatigue resistance of a hot-pressed silicon nitride with magnesia sintering aid is limited by slow crack growth or creep fracture, depending upon the specific stress-temperature conditions. The flexural fracture map is considerably refined relative to earlier versions, and in conjunction with available tension data, was used to create a tension fracture map. The fracture map brings together the findings of a number of studies and can be appreciated by materials scientists and engineers.

U.S. Army Materials Technology Laboratory
Watertown, Massachusetts 02172-0001
FRACTURE MECHANISM MAPS FOR ADVANCED STRUCTURAL CERAMICS. PART I: METHODOLOGY AND HOT-PRESSED SILICON NITRIDE RESULTS - George D. Quinn

Technical Report MTL TR 90-6, February 1990, 30 pp-illus-tables, D/A Project: 1L162105.AH84

AD____________
UNCLASSIFIED
UNLIMITED DISTRIBUTION

Key Words

Ceramics
Silicon nitride
Powders

The static fatigue behavior of advanced structural ceramics can be controlled by a variety of failure mechanisms. A fracture mechanism map can define the stress-temperature regimes where the different mechanisms are dominant. The static fatigue resistance of a hot-pressed silicon nitride with magnesia sintering aid is limited by slow crack growth or creep fracture, depending upon the specific stress-temperature conditions. The flexural fracture map is considerably refined relative to earlier versions, and in conjunction with available tension data, was used to create a tension fracture map. The fracture map brings together the findings of a number of studies and can be appreciated by materials scientists and engineers.